Chair of Reservoir Engineering

Master's Thesis

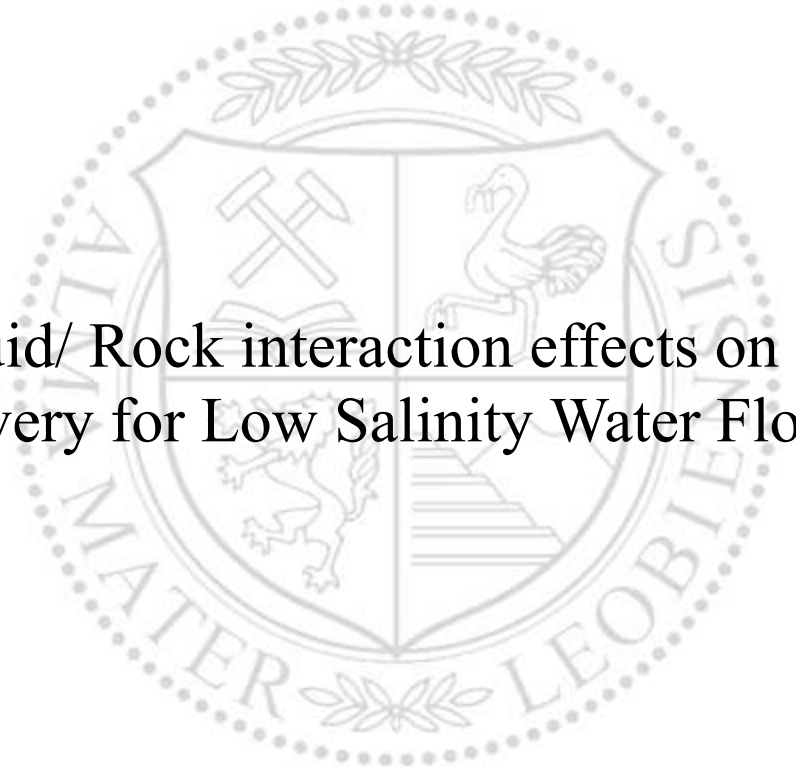

Fluid/ Rock interaction effects on Oil Recovery for Low Salinity Water Flooding

Ahd O A Maguri

September 2021

MONTANUNIVERSITÄT LEOBEN
www.unileoben.ac.at

AFFIDAVIT

I declare on oath that I wrote this thesis independently, did not use other than the specified sources and aids, and did not otherwise use any unauthorized aids.

I declare that I have read, understood, and complied with the guidelines of the senate of the Montanuniversität Leoben for "Good Scientific Practice".

Furthermore, I declare that the electronic and printed version of the submitted thesis are identical, both, formally and with regard to content.

Date 21.09.2021

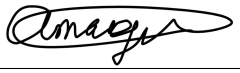

Signature Author
Ahd O A Maguri

Ahd Maguri

Master Thesis 2021

Supervisor: Univ.-Prof. MSc. PhD Riyaz Kharrat

Fluid/ Rock interaction effects on Oil Recovery for Low Salinity Water Flooding

dpe DEPARTMENT PETROLEUM ENGINEERING

MONTAN UNIVERSITÄT

This thesis is dedicated to the memory of my grandfathers

and

My support system – my parents.

Declaration

I hereby declare that except where specific reference is made to the work of others, the contents of this dissertation are original and have not been published elsewhere. This dissertation is the outcome of my own work using only cited literature.

Erklärung

Hiermit erkläre ich, dass der Inhalt dieser Dissertation, sofern nicht ausdrücklich auf die Arbeit Dritter Bezug genommen wird, ursprünglich ist und nicht an anderer Stelle veröffentlicht wurde. Diese Dissertation ist das Ergebnis meiner eigenen Arbeit mit nur zitierter Literatur.

__Ahd O. A. Maguri____

Name, 22 September 2021

Acknowledgments

I would like to express my sincere gratitude to my supervisor Prof. Riyaz Kharrat for his great help, invaluable guidance, and encouragement that helped me throughout my research.

My deep thanks go to OMV Exploration & Production GmbH, for giving me the opportunity to study in Austria.

My extended thanks go to all the members of the Petroleum Engineering Department for an enjoyable two years.

Getting through this work couldn't have been possible without the constant support of my parents, sisters, and close ones, thank you very much.

Abstract

This work has been established based on core flooding data and simulation modeling to investigate the low salinity waterflooding performance and its related mechanisms in carbonate and sandstone reservoirs.

At first, the optimum water composition, ion exchange equivalent fractions, change in mineral moles, and effluent ion concentration have been studied and analyzed on a core scale model. Optimum results of the core scale model were then upscaled for homogenous/ heterogeneous fractured and non-fractured five-spot pilot-scale models. An explicit study of the effect of multi-ion exchange and mineral dissolution/ precipitation was conducted. In addition, the double layer expansion phenomena was investigated implicitly.

The LSWF mechanisms impact was found to be different for the different lithologies. The effluent ion analysis resulted in an increase in the produced Ca^{2+} ion concentration, evidence of mineral dissolution for the sandstone core. For the carbonate core, the reduction of the Ca^{2+} concentration resulted in mineral precipitation. Simulation results showed that the fractional adsorption of the Ca^{2+} ion in the carbonate core was higher than the sandstone, which led to lower recovery for the carbonate core.

In the pilot-scale model, an increase in the potential determining ions (PDIs) were observed in the fractured/ non-fractured homogeneous reservoirs, confirming the calcite and dolomite dissolution, which causes an increase in the pore volume.

Results show that as the Cation Exchange Capacity (CEC) increases, the recovery reduces in the presence of clay since equilibrium requires time with the larger surface area. However, in the absence of clay, CEC has less influence on the recovery.

Finally, based on the studied cores, multi-ion exchange was not the sole mechanism behind LSWF. It requires the support of other mechanisms such as mineral dissolution/ precipitation and double-layer expansion.

Zusammenfassung

Diese Arbeit wurde auf der Grundlage von Kernflutdaten und Simulations Modellierung erstellt, um die Wasserflutleistung mit niedrigem Salzgehalt und die damit verbundenen Mechanismen in Karbonat- und Sandsteinreservoirs zu untersuchen.

Zunächst wurden die optimale Wasserzusammensetzung, Ionenaustauschäquivalentsanteile, Veränderungen der Mineralstoffmenge und die Ionenkonzentration im Abwasser untersucht und anhand eines Kernmodells analysiert. Optimale Ergebnisse des Bohrkernmodells (Kernmaßstab) wurden dann für homogene/heterogene frakturierte und nicht frakturierte Modelle im Pilotmaßstab hochskaliert.

Es wurde eine explizite Studie zum Effekt des Mehrfachionenaustauschs und der Mineralauflösung/Fällung durchgeführt. Außerdem wurden implizit die Doppelschicht-Expansionsphänomene untersucht. Es wurde festgestellt, dass die Auswirkungen des LSWF-Mechanismus für die verschiedenen Lithologien unterschiedlich sind.

Die Ionenanalyse des Abwassers führt zu einer Erhöhung der produzierten Ca^{2+}-Ionenkonzentration, ein Beweis für die Mineralauflösung des Sandsteinkerns. Im Falle des Karbonatkerns, führte die Verringerung der Ca^{2+}-Konzentration zu einer Mineralausfällung. Simulationsergebnisse zeigten, dass die fraktionierte Adsorption des Ca^{2+}-Ionen im Karbonatkern höher war als im Sandstein, was zu einer geringeren Ölgewinnung im Karbonatkern führte.

Im Pilotmodell wurde ein Anstieg der potentialbestimmenden Ionen (PDIs) im frakturierten/nicht frakturierten homogenen Reservoir beobachtet, was die Calcit- und Dolomit-Auflösung, welche eine Zunahme des Porenvolumens verursacht, bestätigt.

Die Ergebnisse zeigen, dass mit zunehmender Kationenaustauschkapazität (CEC) die Ölgewinnung in Gegenwart von Lehm abnimmt, da das Gleichgewicht mit der größeren Oberfläche Zeit braucht. In Abwesenheit von Lehm hat CEC jedoch weniger Einfluss auf die Gewinnung.

Basierend auf den untersuchten Kernen, ist der Mehrfachionenaustausch nicht der Einzige Mechanismus der LSWF. Es erfordert die Unterstützung anderer Mechanismen wie in etwa der Mineralauflösung/Ausfällung und Doppelschichtexpansion.

Table of Contents

Declaration iii
Erklärung iii
Acknowledgments iv
Abstract v
Zusammenfassung vi
Chapter 1 17
Introduction 17
1.1 Background and Context 17
1.2 Scope and Objectives 18
1.3 Achievements 18
1.4 Technical Issues 18
1.5 Overview of Dissertation 19
Chapter 2 21
Literature Review 21
2.1 Rock – Fluid Interactions 21
2.2 Fluid – Fluid Interactions 29
Chapter 3 31
Modeling of Low Salinity Water Flooding in Sandstones & Carbonates 31
3.1 Overview of the related Experiments 33
3.2 Simulation Model Development 33
3.3 Geochemical Reactions 38
3.4 History Matching 40
3.5 Water Optimization 43
3.6 Effect of Ions 44
3.7 Investigation of Low salinity water flooding Mechanisms 45
3.8 Pilot-scale model 46
Chapter 4 49
Results and Discussion 49
4.1 Results Section 49
4.2 Discussion Section 79
Chapter 5 84
Conclusion 84
5.1 Summary 84
5.2 Evaluation 85
5.3 Future Work 85
Chapter 6 87
References 87

List of Figures

Figure 2.1: Conceptual Model describing the DLE mechanism (Elgendy & Porta, 2021) 22
Figure 2.2: Wettability alteration of different phosphate concentrations for core A and B (Hosseini et al., 2021) 25
Figure 2.3: Potential determining ions (PDIs) concentration in inflow and outflow (Saw & Mandal, 2020) 26
Figure 2.4: Dissolution of calcite during LSWF (Saw & Mandal, 2020) 27
Figure 2.5: Reaction rate versus molality of Ca^{2+} (CMG Tutorial, 2020) 28
Figure 2.6: IFT for different water types (Hosseini et al., 2021) 30
Figure 3.1: Study Workflow 32
Figure 3.2: Approach to develop GEM reservoir compositional model for LSWF Core Scale Model 33
Figure 3.3: Core model generated using Builder (CMG) 36
Figure 3.4: History matching oil recovery of 40,000 ppm NaCl water 41
Figure 3.5: Water Oil Relative Permeability curves for 40,000 ppm NaCl water 41
Figure 3.6: History matching field oil recovery of 10,000 ppm NaCl water 42
Figure 3.7: Water Oil Relative Permeability curves for 10,000 ppm NaCl water: from published paper (left) (Pouryousefy et al., 2016) generated from CMG (right) 42
Figure 3.8: Optimization workflow of the injection water 43
Figure 3.9: Flow chart of simulation runs for carbonate and sandstone cores 45
Figure 3.10: Porosity (left) and Permeability (right) in the homogeneous pilot scale model .. 47
Figure 3.11: Random distribution of the Porosity (left) and Permeability (right) in the heterogeneous pilot scale model 48
Figure 3.12: Relative permeability curves in the matrix and fractures for the pilot model 48
Figure 4.1: Coarse salinity range optimization: 1 - 40 K ppm (left) and 40 - 80 K ppm (right) 50
Figure 4.2: Recovery factor comparison between the two coarse salinities and base case 51
Figure 4.3: Recovery factor comparison between coarse, fine range salinities and base case 51
Figure 4.4: Optimization study of the Seawater (SW) using a coarse and fine salinity range 52
Figure 4.5: Relative Permeability in the carbonate rock for high salinity (blue/red) and low salinity (pink/green) 53
Figure 4.6: Optimization runs in the sandstone core with coarse range salinity using only NaCl water as injection water 55
Figure 4.7: Results of optimization study of the NaCl only water using a coarse and fine salinity range compared to the base case 55
Figure 4.8: Results of the Coarse range salinity (left) and Fine range salinity (right) 56
Figure 4.9: Results of optimization study of Seawater (CMG Tutorials, 2018) using a coarse and fine salinity range compared to the base case and NaCl – 1,362 ppm 57
Figure 4.10: Pilot model oil recovery factor in the non-fractured reservoirs 58
Figure 4.11: Pilot model oil recovery factor in the fractured reservoirs 59
Figure 4.12: Depiction of water saturation movement in Heterogeneous reservoir from before water breakthrough (left) to at water breakthrough (right) 60
Figure 4.13: Depiction of water saturation movement in Homogeneous reservoir from before water breakthrough (left) and at breakthrough time of Heterogeneous reservoir (right) 60
Figure 4.14: Sobol Analysis on ion effects impact on the oi recovery in the carbonate rock . 62
Figure 4.15: SO_4^{-2} effect on Oil Recovery for a carbonate core after injecting 1.4 PVs of NaCl water 62
Figure 4.16: Bar chart of oil recovery difference by varying SO_4^{-2} values for a carbonate core after injection 1.4 PVs of NaCl water 63
Figure 4.17: Sobol Analysis on ion impact on the oil recovery in the sandstone rock 64
Figure 4.18: Na^+ effect on Oil Recovery for a sandstone core after injecting 4 PVs of NaCl water 64

Figure 4.19: Bar chart of oil recovery difference by varying Na^+ ion values for a sandstone core after injecting 4 PVs of Seawater 64
Figure 4.20: Mineral Mole change for ions in formation water for carbonate core 65
Figure 4.21: Aqueous Component changes in the carbonate core 66
Figure 4.22: Pore volume change in the carbonate core after 5.4 PVI 66
Figure 4.23: Mineral Mole change for ions in formation water for sandstone core 67
Figure 4.24: Aqueous Component changes in the sandstone core 67
Figure 4.25: Pore volume change in the sandstone core 68
Figure 4.26: Aqueous component change during LSWF in the non-fractured homogeneous reservoir 69
Figure 4.27: Aqueous component change during LSWF in the fractured homogeneous reservoir 69
Figure 4.28: Mineral precipitation in Non-fractured homogeneous reservoir 70
Figure 4.29: Pore volume change from inlet to outlet in the non-fractured homogeneous reservoir 70
Figure 4.30: Mineral Dissolution in the fractured homogeneous reservoir 71
Figure 4.31: Pore volume change from inlet to outlet in the fractured homogeneous reservoir 71
Figure 4.32: Cation concentration during injecting 4,230 ppm optimized seawater in carbonate core 73
Figure 4.33: Adsorption of the divalent cations during injecting 4,230 ppm optimized seawater in carbonate core 73
Figure 4.34: Cation concentration during 1362 ppm NaCl injection 74
Figure 4.35: Adsorption of Ca^{2+} cation during 1,362 ppm NaCl injection 75
Figure 4.36: Cation concentration during 1,362 ppm NaCl injection 75
Figure 4.37: Adsorption of Ca^{2+} cation during 7,670 ppm NaCl injection 76
Figure 4.38: Effect of CEC on the adsorption of the Ca^{2+} ions on the sandstone rock during injection 7,670 ppm water 76
Figure 4.39: Effect of CEC on the oil recovery factor of the sandstone rock with clay during injection 7670 ppm water 77
Figure 4.40: Effect of CEC on the oil recovery factor of the sandstone rock with no clay during injection 7670 ppm water 77

List of Tables

Table 2.1: Important equations for the MIE mechanism (Pouryousefy et al., 2016) 24
Table 3.1: Definition of cases 32
Table 3.2: Core Dimensions for carbonate rock 34
Table 3.3: Experimental data (Bakhshi et al., 2017) 35
Table 3.4: PVT data used in the core model 35
Table 3.5: Composition of the formation water in new case carbonate (Lee et al., 2017) 36
Table 3.6: Mineralogy of carbonate core 36
Table 3.7: Composition of used injection water in the Carbonate core and Sandstone core 37
Table 3.8: Experimental data (Nasralla & Nasr-El-Din, 2014) 37
Table 3.9: Formation Brine Composition (Nasralla & Nasr-El-Din, 2014) 38
Table 3.10: Mineralogy of sandstone core (Nasralla & Nasr-El-Din, 2014) 38
Table 3.11: List of the aqueous, mineral, and ion exchange reactions occurring in a carbonate core 39
Table 3.12: List of the aqueous, mineral, and ion exchange reactions occurring in a sandstone core 40
Table 3.13: Pilot-scale model properties (Kafry, 2020) 47
Table 4.1: Results of coarse salinity range optimization 49
Table 4.2: Results of coarse and fine salinity range optimization of NaCl injection water 50
Table 4.3: Results of coarse and fine salinity range optimization for Seawater optimization 52
Table 4.4: Ion concentration comparison between initial and optimized seawater 53
Table 4.5: Results of base case sandstone 54
Table 4.6: Results of Seawater optimization 56
Table 4.7: Comparison of the results of injecting different waters in sandstone core 57
Table 4.8: Comparison between the composition of the initial and optimized seawater for the new case sandstone 58
Table 4.9: Oil recovery factors for pilot-scale model 61
Table 4.10: Pore Volume change in fracture and matrix system 72
Table 4.11: Comparison of the impact of CEC on recovery for sandstone with and without clay 78
Table 4.12: Cases used to investigate the effect of LSWF on different mineral compositions 78
Table 4.13: Clay effect on recovery in sandstone core 79

Nomenclature

d	diameter	[cm]
k	permeability	[mD]
L	length	[cm]
P	pressure	[psi]
PV	pore volume	[cc]
T	temperature	[F]

Abbreviations

AIMSM	Advanced Ion Management
BP	British Petroleum
CEC	Cation exchange capacity
CMG	Computer Modelling Group
DLE	Double Layer expansion
EDL	Electrical Double layer
EOR	Enhanced Oil Recovery
IFT	Interfacial tension
LSWF	Low salinity water flooding
MIE	Multi-ion exchange
PDI	Potential determining ions

Chapter 1

Introduction

Recent studies have focused on finding a cost-effective, environmentally friendly, and simple enhanced oil recovery (EOR) technique that can alter the crude oil/ brine/ rock interaction, which changes the wettability of the rock to favorable conditions. The alteration of wettability might increase the oil recovery factor in both sandstones and carbonates. Low salinity water flooding (LSWF) is a recent EOR technique that optimizes the injection water's ionic composition and salinity, which results in wettability alteration.

To quantify the impact of LSWF on oil recovery, a geochemical model is used to create a simulation model. The objective is to generate a model through simulation to characterize the impact of the LSWF on fluid and rock properties in the core system and investigate the mechanisms impact on recovery.

Several main mechanisms responsible for oil recovery for the LSWF include double-layer expansion (DLE), multi-ion exchange (MIE), and mineral dissolution/ precipitation. However, so far, the dominant mechanism is still under debate by concerned researchers.

1.1 Background and Context

In this thesis, the main LSWF mechanisms that occur during the injection of a low salinity brine into a carbonate and sandstone core are discussed. In addition, a numerical geochemical reservoir model was built using the Computer Modelling Group (CMG) reservoir simulator based on the experimental data obtained from Bakhshi et al. (2017) for the carbonate core and Nasralla & Nasr-El-Din (2014) for the sandstone core. The aim of this simulation model was to simulate the effect of LSWF and its governing mechanisms on the oil recovery factor for both carbonate and sandstone reservoirs.

1.2 Scope and Objectives

The objective of this work is to study the effects of the low salinity water flooding injection in both sandstone and carbonate rocks by building a numerical simulation model based on the presented experimental data in the literature using Computer Modelling Group (CMG) reservoir simulator. Carbonate reservoirs represent more than 60% of the oil and gas reserves in the world. However, not many studies have been conducted on this lithology due to complexities in characterizing it. This work will focus on making conclusions of the effect of LSWF on both carbonate and sandstone lithologies.

Various LSWF mechanisms such as multi-ion exchange and mineral dissolution/ precipitation impact the oil recovery factor. These mechanisms will be investigated using numerical simulation models based on experimental data. The increase in recovery factor was modeled based on the exchange of potential determining ions (PDIs) in the injection water and the reservoir rocks' surface. The ion exchange equivalent fractions, effluent ion concentration, changes in the mineral moles, pore volume change, and impact of the cation exchange capacity (CEC) have all been explored to determine the dominant mechanism for the specific lithology. In addition, since most carbonate rocks are fractured, in this work, the LSWF has also been implemented on a pilot model to determine its impact on the oil recovery factor in a real case model.

1.3 Achievements

The experimental data of sandstone and carbonated cores were modeled using CMG. Based on the obtained results, no sole LSWF mechanism is responsible for the oil recovery. But instead, a combination of mechanisms such as multi-ion exchange and double layer expansion is accountable. Furthermore, an indication of the governing LSWF mechanism can be determined through effluent ion change analysis. Determining the optimum concentration of the main potential determining ions (PDIs) in the injection water (SO_4^{-2} for the carbonates and Na^+ for sandstones) is essential for obtaining the highest recovery factor from the injection water.

1.4 Technical Issues

The CMG-GEM simulator is a good tool for studying and understanding the LSWF mechanisms, but the simulator had a few shortcomings. CMG-GEM can only model the DLE phenomena' final effects, making it not possible to investigate the oil recovery response to the DLE alone. However, in CMG-GEM, the relative permeability curves are changed to water wet relative permeability curves by employing a relative permeability interpolation to show the

LSWF impact. Basically, in the CMG-GEM wizard, multiple relative permeability sets are created for the interpolation, with the user choosing the interpolant.

1.5 Overview of Dissertation

First, a review of the main LSWF mechanism is given, followed by an introduction to modeling the LSWF effect in carbonates and sandstones based on core experimental data. The steps of building the reservoir model and introducing the geochemical equations activated during the LSWF are discussed. Then, the results obtained from simulations are analyzed. These results give a better understanding of the impact of LSWF on oil recovery. A pilot-scale model was upscaled from core scale data to get an understanding of the LSWF mechanisms in the homogeneous/ heterogeneous fractured and non-fractured reservoirs.

Chapter 2

Literature Review

Understanding the low salinity waterflooding mechanisms in some reservoir rocks such as carbonates is more complicated than others (such as sandstones) due to the complex nature of the carbonate rocks. They depend on the rock mineralogy, injected fluid, and formation water properties. To deeply understand the contribution of the well-known mechanisms such as ion exchange, double layer expansion, a study of the rock-fluid and fluid-fluid interactions is essential. This chapter will summarize and discuss the most important recovery mechanisms in carbonate and sandstone rocks during LSWF.

2.1 Rock – Fluid Interactions

2.1.1 Double Layer Effect (DLE)

The double layer expansion mechanism has been studied by Ligthelm et al. (2009). Their findings stated that during the injection of LSWF, an exponential increase in the electrical potential of the negatively charged component (sandstone rock) and positively charged component in the case of a (carbonate rock) would occur. They introduced this phenomenon as the electrical double layer (EDL). The wettability of the rock might be altered due to the expansion of the EDL resulting from ionic strength reduction. The rock's water wetting increases when the ionic strength decreases because of the bigger separation between the carboxylic material and the rock surface (Tetteh, et al., 2020). This is because the injection of the LSWF causes a disruption in the binding forces, which results in the reduction of the attractive forces. Figure 2.1 shows a conceptual model which describes the double layer expansion (DLE) mechanism.

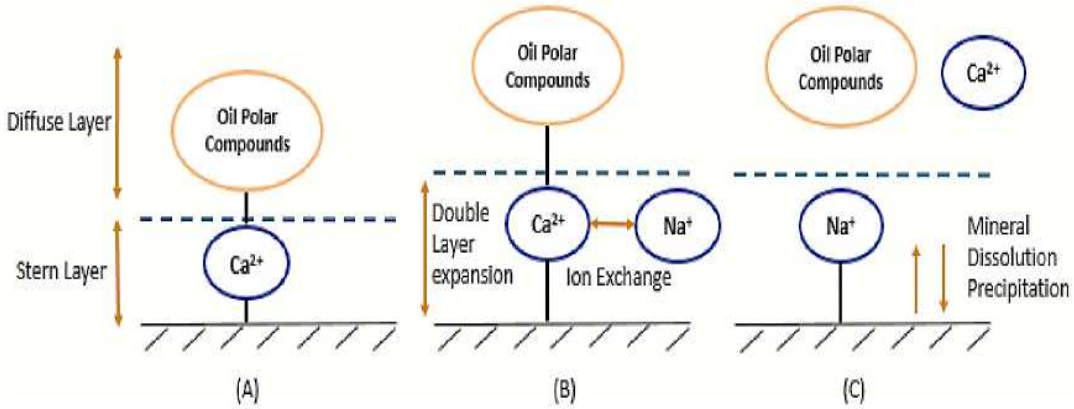

Figure 2.1: Conceptual Model describing the DLE mechanism (Elgendy & Porta, 2021)

The status of the rock-brine interface before injecting LSWF in a sandstone rock is as shown in Figure 2.1(A), which corresponds to a high saline environment. The divalent ion (Ca^{2+}) in the formation water is attached to the negatively charged rock surface and the negatively charged oil polar components. These divalent ions (Ca^{2+} and Mg^{2+}) act as a binding link between the two interfaces and the stern layer. It is closest to the charged rock surface and is relatively small. Upon the LSWF injection, the repulsive forces between the rock surface and oil polar components will increase. This will lead to the expansion of the distance between either interface. The repulsive force will cause the disjoining pressure to be higher than the binding pressure; as a result, a water film which is a thick and stable film, will appear. DLE will facilitate the decrease in the distance between the ion exchangers, which causes the release of the absorbed oil components and hence increase the oil recovery factor, as shown in Figure 2.1 (B).

The conceptual model that describes the effect of DLE in a carbonate rock is like that of a sandstone rock. The difference is that the carbonate rock under reservoir conditions is positively charged, and SO_4^{-2} is the divalent ion responsible for the ion exchange mechanism. DLE cannot be modelled using CMG- GEM because CMG-GEM only models the final effects of the LSWF by switching to the initial oil-wet relative permeability curves to water-wet relative permeability curves through the utilization of the relative permeability interpolations.

2.1.2 Multiple ion exchange (MIE)

Yousef et al. (2011) stated that the main wettability alteration mechanism is multi-ion exchange. The ion exchange between the rock-fluid and fluid-fluid interfaces leads to oil desorption from the rock's surface, altering the wettability (Afekare & Radonjic, 2017). Austad et al. (2015) discussed the importance of SO_4^{-2} ions in the injected fluid; the ions act as surface

neutralizing agents for carbonate rocks (Hosseini, et al., 2021) and can indirectly expel the carboxylate group from the rock surface and hereafter change the wettability of the rock. SO_4^{-2} also absorbs on the rock's surface, decreasing the positive charge on the rock and minimizing the repulsive forces between the cations in the brine and positively charged rock surface.

In sandstone rock, divalent ions such as Ca^{2+} and Mg^{2+} are crucial; they bridge the negatively charged sandstone surface and oil components under reservoir conditions. Once LSWF is injected, and due to the DLE, the distance between these negatively charged interfaces increases. As a result, the absorbed oil is released, resulting in an increase in the oil recovery factor (Zhang, et al., 2007). Based on the affinity of divalent ions towards the clay surface, the MIE process can cause these divalent cations to absorb on the rock surface until the cation exchange capacity (CEC) of the rock is reached (full saturation), as shown in Figure 2.1 (B). For example, Ca^{2+} has a higher affinity to be absorbed on the rock's surface than Mg^{2+} so that it can replace it during the MIE process.

For carbonate rocks, the SO_4^{-2} has an important role in wettability alteration compared to other negative ions such as Cl^-, which has a negligible effect on wettability alteration. This could be due to; electronegativity. SO_4^{-2} ions have a higher tendency to share negative ions. Also, it has an ionic charge of minus two, which is very important in DLE and MIE. Another reason which Hosseini et al. (2021) observed to be the most important is the geometric shape of the SO_4^{-2} ion.

Ion exchange reactions are modeled as chemical equilibrium reactions. Because the reactions between the components in the aqueous phase are fast relative to the reactions that occur during mineral dissolution/ precipitation. This process can be converted into geochemical equations, which are input for the simulator and are shown in Table 3.11 and Table 3.12. "X" is the clay mineral (ion exchanger on the sandstone surface) that has the divalent ion (Ca^{2+} or Mg^{2+}) attached to it, corresponding to Figure 2.1 (A). Once the low salinity water is injected, there is an ion exchange between the divalent ion (Ca^{2+} or Mg^{2+}) and monovalent Na^+. The Na^+ is now attached to the rock. The divalent ions are released, meaning there will be a decrease of divalent ions in the system, indicating the MIE mechanism. In a reservoir with temperatures higher than 90 degrees Celsius, Mg^{2+} has a higher tendency (higher affinity towards the clay surface) to replace the Ca^{2+} ions, so Mg-X2 will be used as the interpolant for modelling the relative permeability curve changes at higher reservoir temperatures (Zhang, et al., 2007).

The ions involved in the reactions are important to distinguish between the adsorption of the organic matter due to MIE and DLE. A major difference between the two mechanisms is that only monovalent cations contribute during DLE, whereas the divalent ions interact with both MIE and DLE. It is important to analyze the effluent ion changes because alteration in the PDIs

can indicate the working mechanism. According to literature, a decrease in Ca^{2+} indicates MIE (Awolayo, 2014; Chandrasekhar, 2018). In contrast, an increase in the production of the Ca^{2+} is an indication of dissolution effects (Hadi, et al., 2019).

Equilibrium reactions can be used to describe the adsorption of organic material by different mechanisms. The equilibrium reaction, selectivity coefficient, and cation exchange are given in Table 2.1 (Nghiem, et al., 2004).

Table 2.1: Important equations for the MIE mechanism (Pouryousefy et al., 2016)

Equation Name	**Equation**	
Equilibrium reaction	$\text{Log}(K_{eq}) = a_0 + a_1 T + a_2 T^2 + a_3 T^3 + a_4 T^4$	Equation 2.1
Selectivity Coefficient	$K'_{Na/Ca} = \frac{\xi(Na-X)[m(Ca^{2+})]^{0.5}}{[\zeta(Ca-X2)]^{0.5} m(Na^{+})} \times \frac{[\gamma(Ca^{2+})]^{0.5}}{[\gamma(Na^{+})]}$	Equation 2.2
Cation Exchange Capacity (CEC)	$VN_{Na\text{-}X2} + 2VN_{Ca\text{-}X2} + 2VN_{Mg\text{-}X2} = V\varphi\ (CEC)$	Equation 2.3

In CMG, the selectivity coefficients are used instead of activity coefficients to calculate the activity of the products in the chemical equilibrium equations. This is due to the challenges in calculating the activity coefficient. Selectivity coefficient is "*the degree to which an ion-selective electrode responds to a particular ion with respect to a reference ion"* (Appelo & Postma, 2005). The selectivity coefficient for the Na^{+} and Ca^{2+} reactions are defined in Table 2.1 by Equation 2.2. The selectivity coefficient values used in CMG are based on experimental data, and they are predefined.

The Cation Exchanger Capacity (CEC) needs to be introduced to determine the number of ions adsorbed onto the rock surface. It is an important property of the ion exchanger (X), as described by Equation 2.3 in Table 2.1. Equation 2.3 must be satisfied because CEC is a measurable rock property. It is another necessary input parameter to the simulator, and it is the maximum value of ions allowed on the rock's surface.

Phosphate ($H_2PO_4^{-}$) is an ion with a similar geometric shape and electronegativity of its atoms to sulfate (SO_4^{-2}). The SO_4^{-2} ion was replaced with $H_2PO_4^{-}$, to emphasize its role in the wettability process by Hosseini et al. (2021). It should be noted that $H_2PO_4^{-}$ has similar electrostatic behavior as $SO_4^{-2.}$ They prepared three different smart water compositions of

SW2000 (seawater diluted to TDS= 2000 mg/L) with three different phosphate concentrations, which are as follows:

1) SW0.5S: phosphate concentration is half of sulfate,
2) SW1S: phosphate concentration is equal to sulfate,
3) SW2S: phosphate is double the sulfate concentration.

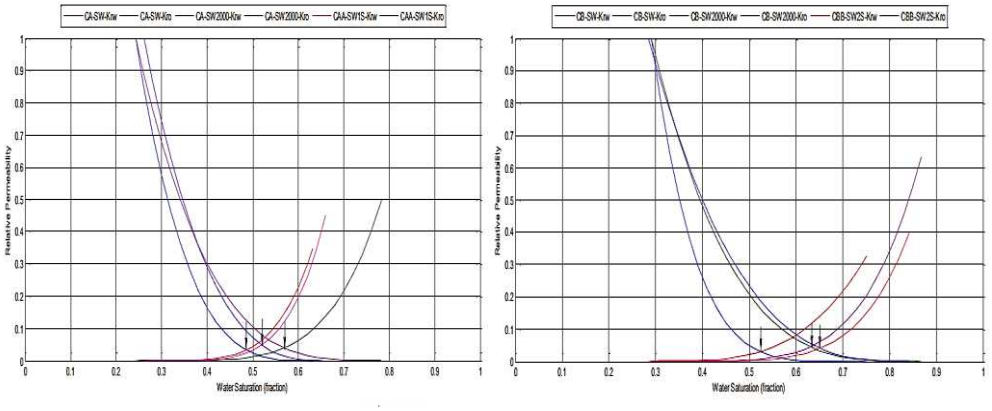

Figure 2.2: Wettability alteration of different phosphate concentrations for core A and B (Hosseini et al., 2021)

This was done to study the effect of substituting sulfate with phosphate. Relative permeability curves were compared using four different cores: core A, core AA, core B, and core BB. When using equal concentrations of SO_4^{-2} and $H_2PO_4^-$, it was observed that SO_4^{-2} is more negatively charged.

From Figure 2.2 it can be summarized that the highest wettability alteration was observed in core B (CB) by using a phosphate concentration that is double the sulfate (SW2S). This is due to the amount of negative charge that is double the amount regarding the SW2000 case. However, SW2000 had a higher wettability alteration than the case of SW1S. This also had to do with the charges. The phosphate has one negative charge, whereas the sulfate has two. This means that the sulfate would alter the surface charge of the rock more than the case of using SW1S.

2.1.3 Mineral Dissolution / Precipitation

When CO_2 dissolves in water, it forms carbonic acid. The reaction of this acid with the rock minerals disrupts the system's equilibrium, leading to mineral dissolution. A 19% total oil incremental recovery was achieved by injecting diluted seawater in limestone core (Yousef, et al., 2011). The pressure drop decrease caused by the carbonate rock dissolution changes the pore geometry.

Hadi et al. (2019) conducted an experiment related to the dissolution effect to permeability and porosity alteration. As dissolution occurs, the pores are enlarged, causing a permeability/ porosity increase. Mahani et al. (2015) stated that the low salinity waterflooding could occur without the effect of dissolution since the major mechanism is wettability alteration.

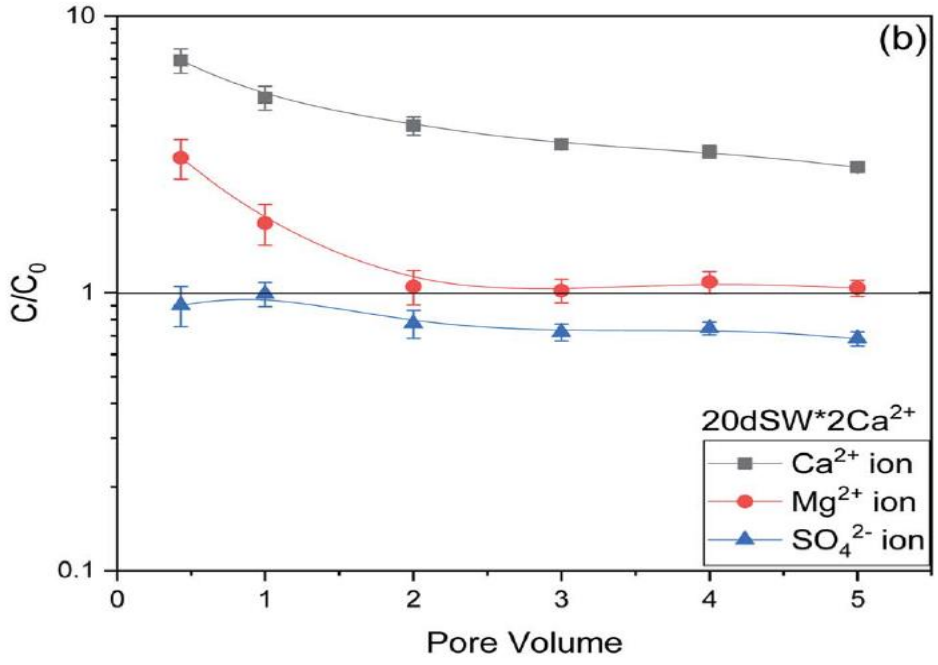

Figure 2.3: Potential determining ions (PDIs) concentration in inflow and outflow (Saw & Mandal, 2020)

Saw & Mandal (2020) suggested that the lower salinity injected water disturbs the equilibrium once present during high saline conditions during seawater dilution. This causes the ions on the rock surface to dissolve due to the low salinity injected water. The produced Ca^{2+} ions concentration increase indicates the dissolution effects (Hadi, et al., 2019). As shown in Figure 2.3, the concentration of the Ca^{+2} ions is much higher at the outflow than the injected brine. This is an indication of calcite dissolution. Saw & Mandal (2020) concluded that the main mechanism that results in oil recovery due to seawater dilution is the calcite dissolution and the effect of positive determining ions during the multi-ionic exchange.

During the ion exchange, the carboxylic materials previously absorbed onto the rock surface are now desorbed, resulting in the possibility of mineral dissolution and precipitation incrementally, as shown in Figure 2.1(C). Figure 2.4 shows a schematic depiction of the dissolution of calcite as the potential determining ions (PDIs) in the injection water are altering the wettability of the rock from originally oil wet to water wet, which is the favorable wettability condition of the rock.

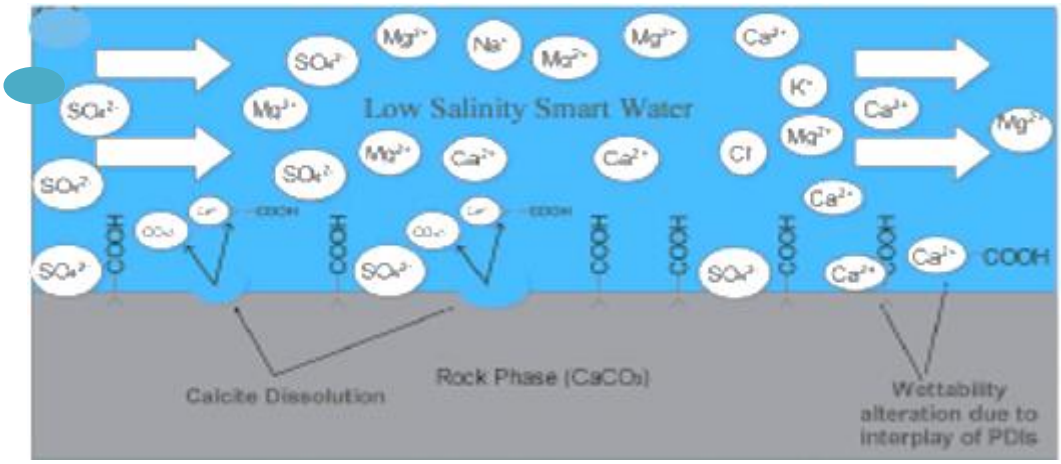

Figure 2.4: Dissolution of calcite during LSWF (Saw & Mandal, 2020)

Dissolution causes the bond between the rock surface and minerals to break, which leads to fine mobilization (Hadi, et al., 2019). When the mobilized fines flow in the system, they cause blockage of pore-throats, diverting the flow to un-swept zones in the reservoir. This results in an improved volumetric sweep efficiency and hence an oil recovery increase. When fine migration and dissolution coexist, no change in permeability might be witnessed. Fine migration causes a permeability reduction due to blockage of pores, whereas dissolution results in a permeability increase. These effects can be further visualized using the CMG-GEM software package.

Austad et al. (2015) focused on the importance of the presence of anhydrite in the rock mineralogy because anhydrite dissolution will create an additional source of SO_4^{-2}. However, other studies conducted on carbonates with no anhydrite still showed recovery improvements.

2.1.3.1 Effects of mineral precipitation/dissolution using CMG-GEM

The modeling approach for the CMG-GEM software package includes mineral dissolution/ precipitation reactions that describe the changes in porosity and permeability that occur during low salinity injection. These types of reactions are rate-dependent and thus are relatively slow in comparison to the chemical equilibrium reactions. The simulator has two main controlling mineral reactions that categorize the reaction based on the saturation index (CMG Tutorial, 2020).

1. When the saturation index (qb/keq) is > 1 the reaction is a forward reaction (mineral dissolution),
2. When the saturation index (qb/keq) is < 1 the reaction is a backward reaction (mineral precipitation).

The mineral dissolution and precipitation reactions are shown in Table 3.11 and Table 3.12. The precipitation mechanism of calcite is described in Equation 3.1. The calcite precipitation

process during LSWF occurs when the CO_2 dissolved in the water forms HCO_3^- when the Ca^{2+} ions are in excess, it causes the previous equation to shift to the left side, and this causes calcite to precipitate (Esene, et al., 2018).

As for the dissolution, LSWF favors the dissolution of the dolomite mineral in the carbonate rock. Equation 3.2 describes this mechanism for dolomite. It occurs when there is an excess of H+ and a deficiency in the HCO_3^- and Ca^{2+}, resulting in the equation moving towards the right side to dissolve more dolomite. CMG cannot calculate the equilibrium rate; however, when the precipitation and dissolution are insignificantly small, it will not have a big impact on any porosity, permeability, or pore volume changes.

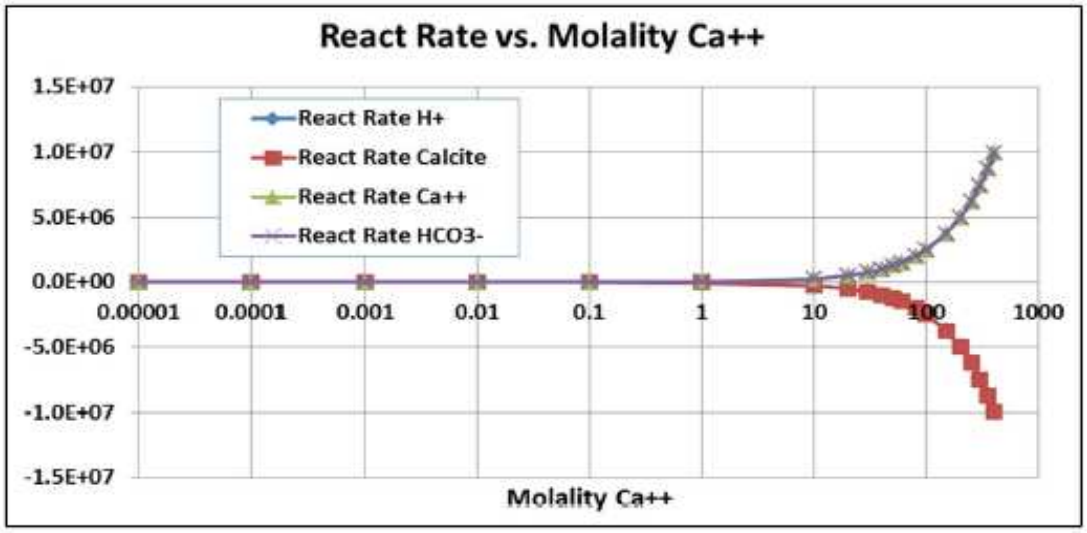

Figure 2.5: Reaction rate versus molality of Ca^{2+} (CMG Tutorial, 2020)

Figure 2.5 is from a CMG tutorial; it shows that the higher the molality of the Ca^{2+} ion, the higher the reaction rate (qb). In addition, as the molality of the Ca^{2+} (product) ion increases, the calcite (reactant) reaction rate decreases. This means a forward reaction is present; hence mineral dissolution is present.

According to Austad et al. (2015), the upper limit of low salinity is 5000 ppm TDS. However, according to Hosseini et al. (2021), if the water is further diluted, it can also result in higher recovery due to further wettability alteration.

Recently the injection configuration scheme has been shown to improve oil recovery. Hosseini et al. (2021) concluded that using high salinity water injection after low salinity water injection will provide an incremental oil recovery making it the better procedure to take. One more observation was the high presence of non-active ions. Based on these observations, it has been proposed that using high salinity after a low water salinity water flooding increases the ionic

concentration at the surface and decreases the diffuse layer thickness due to the presence of non-active ions.

2.2 Fluid – Fluid Interactions

2.2.1 Water in oil microemulsions

The formation of microemulsions was observed to improve the oil recovery by altering rock wettability to more water-wet. It has been suggested that the microemulsion was formed by the presence of the natural surfactants in the oil and oils with a high TAN number (Emadi & Sohrabi, 2013). Tetteh et al. (2020) proposed that during low salinity water flooding, the intermolecular forces that hold the oil-brine interface become weak, resulting in the water molecules moving into the oil phase and interacting with the surfactant, creating the microemulsions then altering the wettability. Sandengen et al. (2016) suggested that during LSWF, these microemulsions were formed due to the osmotic gradient between the high salinity connate water and the low salinity injection water. However, no additional recovery was observed based on the core flooding experiment by Tetteh et al. (2020). During the core flood experiment using oil without the natural surfactant, microemulsions did not form. This caused a negative effect on the oil recovery, concluding that the presence of these natural surfactants in the crude oil is crucial for improving the oil recovery (Tetteh, et al., 2020).

2.2.2 Interfacial tension reduction

During a waterflood, the two most important mechanisms that occur to enhance the oil recovery are wettability alteration and IFT reduction. IFT alteration is triggered by a change in water composition (Hosseini, et al., 2021). An increase in the pH during the LSWF causes a wettability alteration. McGuire et al. (2005) suggested that an improvement in capillary number occurs when the IFT decreases between the oil and brine, caused by this pH level increase. However, others did not observe a significant IFT decrease to improve the capillary number (Yousef, et al., 2011).

IFT reduction occurs when the polar head of the carboxyl oil absorbs cations such as Mg^{2+} and Ca^{2+} in the brine because of its negative charge. The anions such as Cl^- s job is to disturb the surface, so when the low salinity water is injected, the anions start to gain more freedom, resulting in more cations to attract the carboxyl material. This results in IFT reduction between the oil and brine phase. However, as seen in Figure 2.6, the relationship between IFT reduction and water dilution is non-monotonic; IFT reduction will not continue with a further dilution of the water. There is a threshold salinity in which IFT will not reduce but will rather increase, making it important to focus on the IFT change for each recovery process.

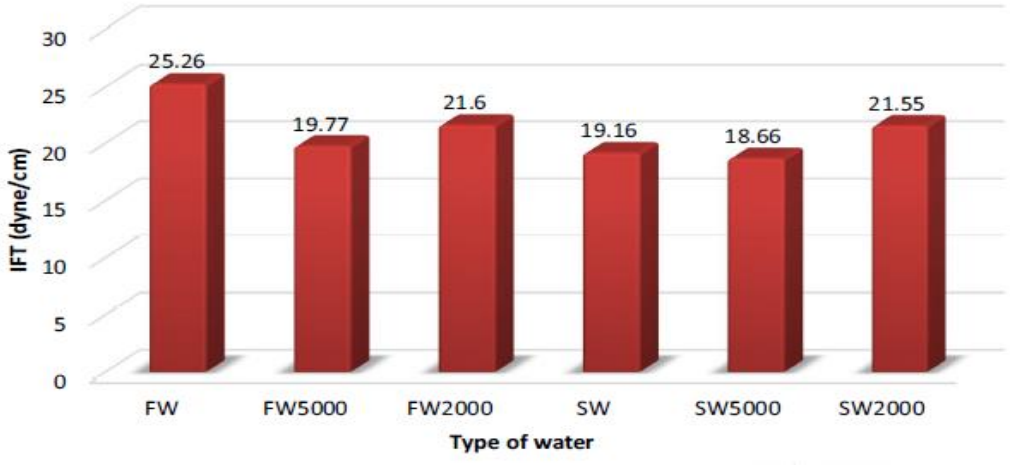

Figure 2.6: IFT for different water types (Hosseini et al., 2021)

Chapter 3

Modeling of Low Salinity Water Flooding in Sandstones & Carbonates

Two compositional models were developed using CMG packages. CMG- WinProp was used to build the fluid model, CMG-Builder was used to build the core model, CMG- GEM was used to simulate the compositional model, and CMG-CMOST, an optimization, and sensitivity analysis generator were used. The workflow shown in Figure 3.1 shows the methodology followed for this study. Firstly, a compositional model was created based on the experimental data (a detailed workflow of the procedure is shown in Figure 3.2). Next, the model was validated by history matching. After that, the water composition was optimized for the base case carbonate and base case sandstone cases. Once the water flood model was established, the optimization study was conducted on the new case carbonate and new case sandstone cases (all the cases are defined in Table 3.1). Furthermore, a study of the impact of specific ions on the recovery factor, in addition to the investigation of the LSWF mechanisms was conducted. Finally, the core model was upscaled to a homogeneous/ heterogeneous fractured/ non-fractured pilot model in which the optimum seawater was injected.

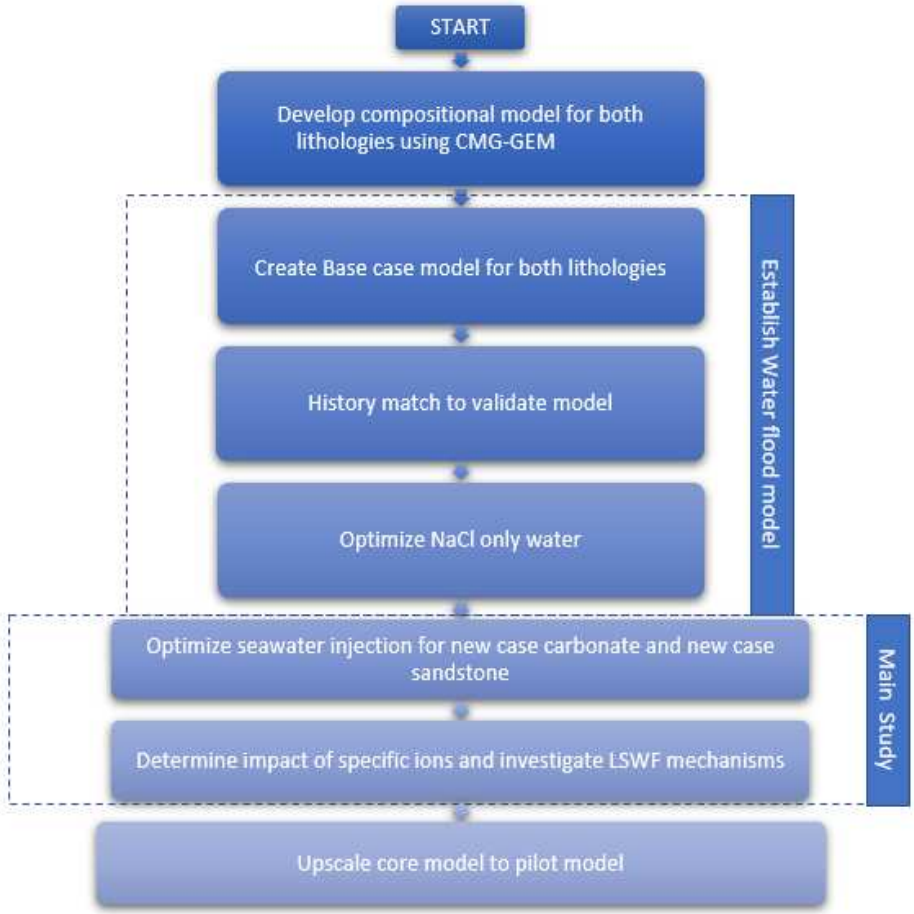

Figure 3.1: Study Workflow

Table 3.1: Definition of cases

Case Name	Formation Water Salinity (ppm)	Injection Water Salinity (ppm)
Base case carbonate	40,000 NaCl only	40,000 NaCl only
Base case sandstone	174,156 (Nasralla & Nasr-El-Din, 2014)	10,000 NaCl only
New case carbonate	26,958.1 (Lee et al., 2017)	41,964 Seawater (CMG Tutorials, 2018)
New case sandstone	174,156 (Nasralla & Nasr-El-Din, 2014)	41,964 Seawater (CMG Tutorials, 2018)

3.1 Overview of the related Experiments

A numerical simulation was performed to study low salinity water flooding (LSWF) performance in carbonate and sandstone rocks. This was done by using Bakhshi et al., (2017) experimental core flood data to study its impact on carbonate rocks and Nasralla & Nasr-El-Din's (2014) data to study its impact on sandstone rocks.

For the carbonate core, Bakhshi et al. (2017) studied the effects of injecting water with 40,000 ppm salinity into a formation with the same salinity; it presented a recovery factor of 36.5%. The SO_4^{-2} ion is used as an interpolant to model the effects of LSWF in a carbonate rock made of 50% calcite and 50% dolomite. One of the drawbacks of simulating LSWF using CMG is that only $SO4^{-2}$ and Ca^{2+} can be used as interpolants for carbonates. This could be challenging when simulating LSWF in very heterogeneous or fractured reservoirs (Esene, et al., 2018).

As for the sandstone core, Nasralla & Nasr-El-Din (2014), data was used to simulate the effects of LSWF by injecting either NaCl or $CaCl_2$ by using various salinities to understand the interaction between the injection fluid and the rock.

3.2 Simulation Model Development

The simulation workflow followed to obtain the fluid and rock properties to conduct the simulations for both rock types is summarized in Figure 3.2.

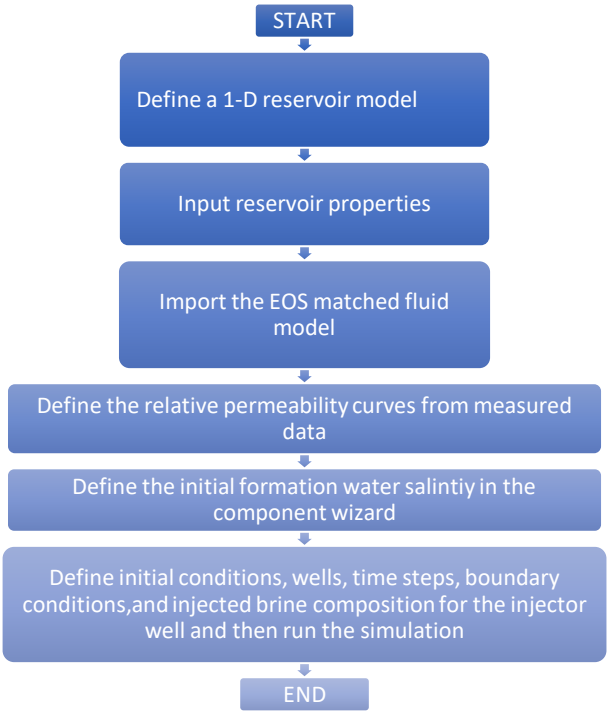

Figure 3.2: Approach to develop GEM reservoir compositional model for LSWF Core Scale Model

3.2.1 Carbonate Core Modelling

In this work, a compositional model is built using the CMG-GEM package to study the impact of LSWF in carbonates implementing it on a base case carbonate model (defined in Table 3.1). It includes injecting only NaCl water to establish the waterflood model and then implementing it on the new case carbonate model.

Then the $SO4^{-2}$ concentration is altered to find the critical $SO4^{-2}$ value and its impact on the oil recovery. $SO4^{-2}$ is assumed to have the most impact on LSWF in carbonate cores. It can promote Ca^{2+} ions' adsorption through $CaSO_4$ production and the desorption of the negatively charged carboxylic components (R-COO-). This increases the oil mobility and hence oil recovery (Zhang & Austad, 2006).

Steps taken to develop the model are summarized in Figure 3.2. The first step is defining the one-dimensional reservoir grid. The data published by Bakhshi et al. (2017) was used to create a one-dimensional core-flooding model built-in CMG to simulate the effects of LSWF in carbonate rocks. The grid model dimensions of the core are shown in Table 3.2. A core with a length of 14.48 cm is considered with 100 grids is used in the I direction and one grid in the J and K.

The next step is to input reservoir properties such as core, oil, and water, shown in Table 3.3. These properties, in addition to the output results, will be used in the simulation work. Furthermore, the matched fluid model obtained from WINPROP, which provides PVT data such as lumped oil components, reservoir temperature, and pressure, are shown in Table 3.4.

Table 3.2: Core Dimensions for carbonate rock

Core Dimensions			
	I	J	K
Number of Cells	100	1	1
Dimensions of Each Cell (m)	0.001448	0.03354	0.03354

Table 3.4 shows the list of the lumped oil components generated using one of CMG packages (WINPROP), a fluid property characterization tool (CMG). Once the fluid model is generated, it is inserted into the core model, created using (BUILDER), another CMG package. The generated core model, which is used to study the effects of LSWF, is shown in Figure 3.3.

Table 3.3: Experimental data (Bakhshi et al., 2017)

Core Properties					
D (cm)	L (cm)	PV (cc)	K (md)		Porosity
3.785	14.48	15.6	0.901		0.096
Oil Properties					
API	Density (g/cc)	Viscosity (cp)	T (F)		P (psi)
33.8	0.8277	0.4168	140		2000
Water Properties				RF (%)	Injected - PV
NaCl (ppm)	Injection Rate (m^3/day)	Viscosity (cp)	NaCl-Water	39.74	1.4
40,000	0.000144	0.63			

Table 3.4: PVT data used in the core model

PVT Data	
P (psi)	2000
T (F)	140
Composition	Mole Fraction
CO_2	0.00080
H_2S	0.00010
N_2	0.00560
C1 to C3	0.08769
IC4 to NC5	0.15998
FC6	0.74483
Total	1.00

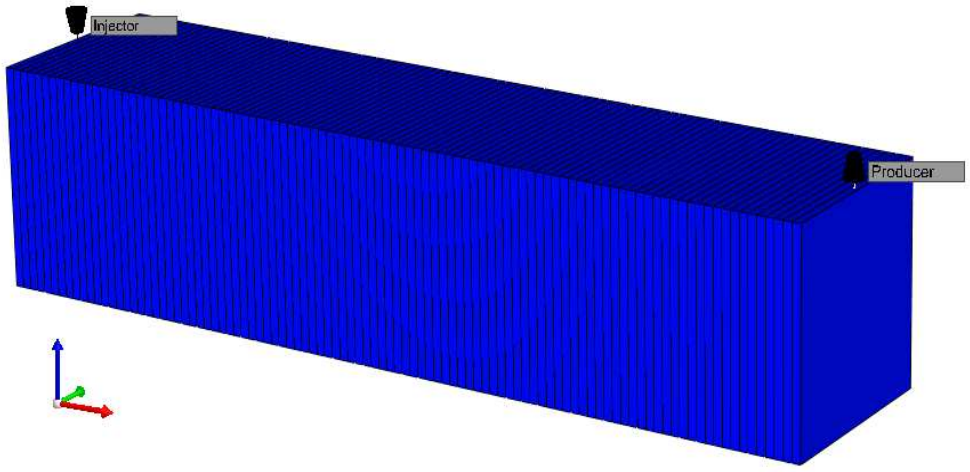

Figure 3.3: Core model generated using Builder (CMG)

The base case carbonate formation salinity is 40,000 NaCl, and the formation water salinity of the new carbonate case is 26,958,1 ppm (Table 3.5). The mineral composition of the carbonate core is shown in Table 3.6. Table 3.7 shows the injected seawater composition, which was used for both carbonate and sandstone rocks.

Table 3.5: Composition of the formation water in new case carbonate (Lee et al., 2017)

	Ca^{2+} (ppm)	Mg^{2+} (ppm)	Na^{+} (ppm)	Cl^{-} (ppm)	HCO_3^{-} (ppm)	SO_4^{2-} (ppm)	Sum (ppm)
Formation Water (FW)	320.4	329	9615	15,117.2	1135.9	550.6	26,958.1

Table 3.6: Mineralogy of carbonate core

Minerals	BBS (wt%)
Calcite	50
Dolomite	50

Table 3.7: Composition of used injection water in the Carbonate core and Sandstone core

	Ca^{2+} (ppm)	Mg^{2+} (ppm)	Na^{+} (ppm)	Cl^{-} (ppm)	HCO_3^{-} (ppm)	SO_4^{2-} (ppm)	Sum (ppm)
Seawater (CMG Tutorials, 2018)	511	1,540	13,200	23,400	163	3,150	41,964

3.2.2 Sandstone Core Modelling

The core model used in the simulation for the sandstone core is identical to that of the carbonate core and is shown in Figure 3.3. The experimental data are summarized in Table 3.8. The formation brine composition used in the study is summarized in Table 3.9, and the mineralogy of the sandstone rock is shown in Table 3.10.

Table 3.8: Experimental data (Nasralla & Nasr-El-Din, 2014)

Core Properties				
D (cm)	L (cm)	PV (cc)	K (md)	Porosity
3.785	14.48	25	111.1	0.182
Oil Properties				
Density (g/cc)	Viscosity (cp)	T (°F)	P (psi)	
0.820	3.7	212	1000	
Water Properties				RF (%)	Injected - PV
NaCl (ppm)	Injection Rate (m3/day)	Viscosity (cp)	NaCl-Water	82	12
10,000	0.00072	0.63			

Table 3.9: Formation Brine Composition (Nasralla & Nasr-El-Din, 2014)

	Ca^{2+} (ppm)	Mg^{2+} (ppm)	Na^{+} (ppm)	Cl^{-} (ppm)	HCO_3^{-} (ppm)	SO_4^{2-} (ppm)	Sum (ppm)
Formation Water (FW)	10,600	1610	54,400	107,000	176	370	174,156

Table 3.10: Mineralogy of sandstone core (Nasralla & Nasr-El-Din, 2014)

Minerals	BBS (wt%)
Quartz	85.0
Feldspar	6.4
Calcite	2.8
Illite	2.0
Kaolinite	3.8

3.3 Geochemical Reactions

The geochemical reactions might occur in three main groups: aqueous, ion-exchange, and mineral dissolution/precipitation. These reaction groups can be classified based on reaction speed into reaction models; aqueous and ion exchange reactions are rather fast, so they are classified as chemical equilibrium reactions, whereas mineral dissolution /precipitation is slow, so they are classified as rate-dependent reactions.

For the ion exchange equations, there is an interaction occurring between a mobile phase and stationary phase. The stationary phase (X), which is the ion exchanger on the rock surface, and ($Ca\text{-}X_2$) and (Na-X) are the equivalent fraction of the ions on the exchanger (Pouryousefy, et al., 2016). The mobile phase is the released or absorbed ion. This is a reversible reaction. When low salinity water is injected into a formation, Ca^{2+} is absorbed onto the free rock surface, and Na^{+} is released. However, when high salinity water is injected, the opposite occurs. The type

of geochemical reactions occurring for both carbonate and sandstone cores are discussed in the following section:

3.3.1 Carbonate Core

The composition of the carbonate core model is 50 % dolomite and 50 % calcite. The geochemical equations that describe the mineral dissolution/ precipitation are known as rate-dependent reactions. They account for the change in the rock minerals and determine the effects of the reactions on the carbonate core during low salinity injection. In addition, the second type of geochemical reaction occurring is the aqueous reaction. These reactions are chosen based on the mineral composition of the rock. Aqueous reactions account for the interaction between the water and CO_2; they are spontaneous and are represented as equilibrium reactions. For a carbonate rock made from dolomite and calcite, the geochemical equations used are shown in Table 3.11.

Table 3.11: List of the aqueous, mineral, and ion exchange reactions occurring in a carbonate core

Mineral Reactions	
$Calcite + H^+ \leftrightarrow Ca^{2+} + HCO_3^-$	Equation 3.1
$Dolomite + 2(H^+) \leftrightarrow Ca^{2+} + 2(HCO_3^-) + Mg^{2+}$	Equation 3.2
Aqueous Reactions	
$Co_2\,(aq) + H_2O \leftrightarrow H^+ + HCO_3^-$	Equation 3.3
$H^+ + OH^- \leftrightarrow H_2O$	Equation 3.4
$CaHCO_3^+ \leftrightarrow Ca^{2+} + HCO_3^-$	Equation 3.5
$CaSO_4 \leftrightarrow Ca^{2+} + SO_4^{2-}$	Equation 3.6
$MgSO_4 \leftrightarrow Mg^{2+} + SO_4^{2-}$	Equation 3.7
$HSO_4^- \leftrightarrow H^+ + SO_4^{2-}$	Equation 3.8
$NaCl \leftrightarrow Na^+ + Cl^-$	Equation 3.9
Surface Charge Alteration Reaction	
$SO_4^{2-} + 2R\text{-}COO\text{-}X = 2\ R\text{-}\ COO\text{-} + SO_4 - X_2$	Equation 3.10

3.3.2 Sandstone Core

Calcite is a mineral that is quite volatile, which means that it is expected to dissolve in the formation water quite easily (Pouryousefy, et al., 2016). The sandstone core has several minerals in its composition, so the mineral reactions occurring during the LSWF are shown in Table 3.12.

Table 3.12: List of the aqueous, mineral, and ion exchange reactions occurring in a sandstone core

Mineral Reactions	
Quartz = SiO_2	Equation 3.11
K-feldspar + 4(H+) = (Al+++) + 2H2O +(K+) + 3SiO_2	Equation 3.12
Calcite + $H^+ \leftrightarrow Ca^{2+} + HCO_3^-$	Equation 3.13
Illite + 8 (H+) = 2.3 (Al+++) + 5H2O + 0.6(K+) +0.25(Mg++) + 3.5 SiO_2	Equation 3.14
Kaolinite + 6(H) = 2(Al+++) + 5H2O + 2SiO_2	Equation 3.15
Aqueous Reactions	
Co_2 (aq) + $H_2O \leftrightarrow H^+ + HCO_3^-$	Equation 3.16
$H^+ + OH^- \leftrightarrow H_2O$	Equation 3.17
Ion Exchange Reactions	
Na + 0.5 Ca – X_2 = 0.5 Ca_2 + Na – X_1	Equation 3.18
Na + 0.5 Mg – X_2 = 0.5 Mg_2 + Na – X_1	Equation 3.19

3.4 History Matching

3.4.1 Carbonate Core

The model generated by CMGs pre-processor Builder was exported into the compositional simulator (GEM). Several scenarios were generated; in the base case carbonate model, 1.4 PVs of 40,000 ppm, only NaCl water was injected into the rock with formation water salinity of 40,000 ppm. History matching between simulation and experimental data was conducted to

validate the model to make further studies. It was conducted using the CMG- CMOST software package. Several simulation cases are created and compared with the experimental data until an optimum case with the lowest global error is found. The history matched oil recovery is shown in Figure 3.4. After history matching, the obtained recovery factor was 38.97%.

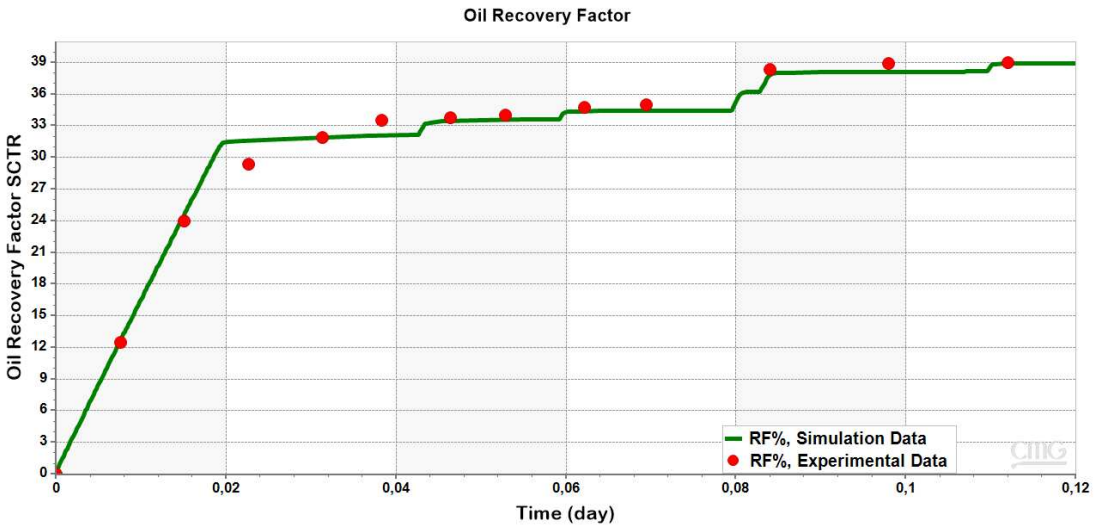

Figure 3.4: History matching oil recovery of 40,000 ppm NaCl water

From history matching, the relative permeability curves will be altered to match those of the experimental data. The resultant relative permeability curves which will be used in this study are shown in Figure 3.5.

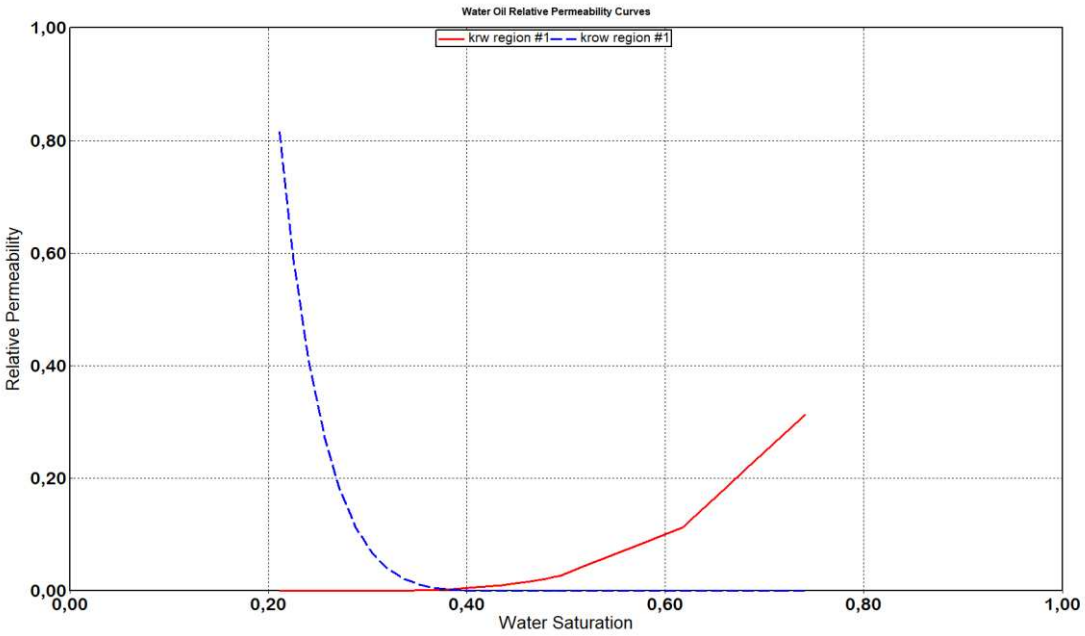

Figure 3.5: Water Oil Relative Permeability curves for 40,000 ppm NaCl water

3.4.2 Sandstone Core

The model generated by CMGs pre-processor Builder was exported into the compositional simulator (GEM). Several scenarios were generated; in the base case sandstone, only NaCl water with a salinity of 10,000 ppm was injected into the sandstone rock to displace the oil with the formation water salinity composition shown in Table 3.9. History matching between simulation and experimental data was conducted to validate the model to make further studies. The history matched oil recovery is shown in Figure 3.6. After history matching, the obtained recovery factor was 81.3 %.

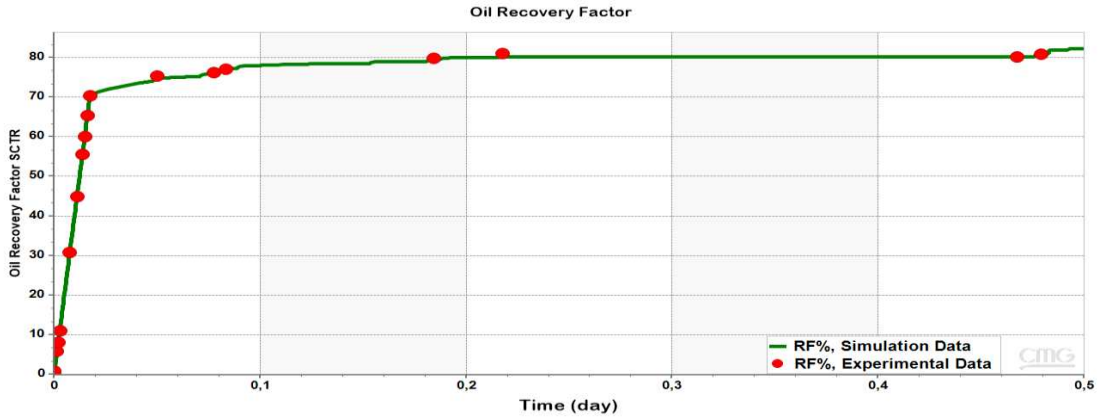

Figure 3.6: History matching field oil recovery of 10,000 ppm NaCl water

From history matching, the relative permeability curves will be altered to match those of the experimental data. The resultant relative permeability curves which will be used in this study are shown in Figure 3.7.

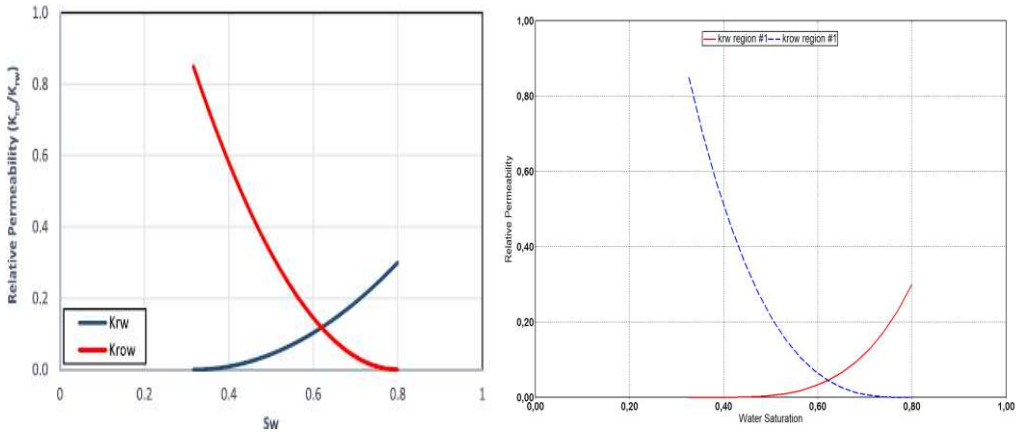

Figure 3.7: Water Oil Relative Permeability curves for 10,000 ppm NaCl water: from published paper (left) (Pouryousefy et al., 2016) generated from CMG (right)

3.5 Water Optimization

Water optimization is done to investigate the possibility of injecting a brine with a salinity different from the base case, resulting in a higher recovery factor. A statistical approach will be followed for this optimization, and its workflow is shown in Figure 3.8. For this optimization, the CMG-CMOST package is used. It works by setting a coarse and fine range of salinities for the injection water. Firstly, the coarse salinity range is used. Once the optimum concentration is obtained, a finer salinity range is simulated to obtain more accurate results.

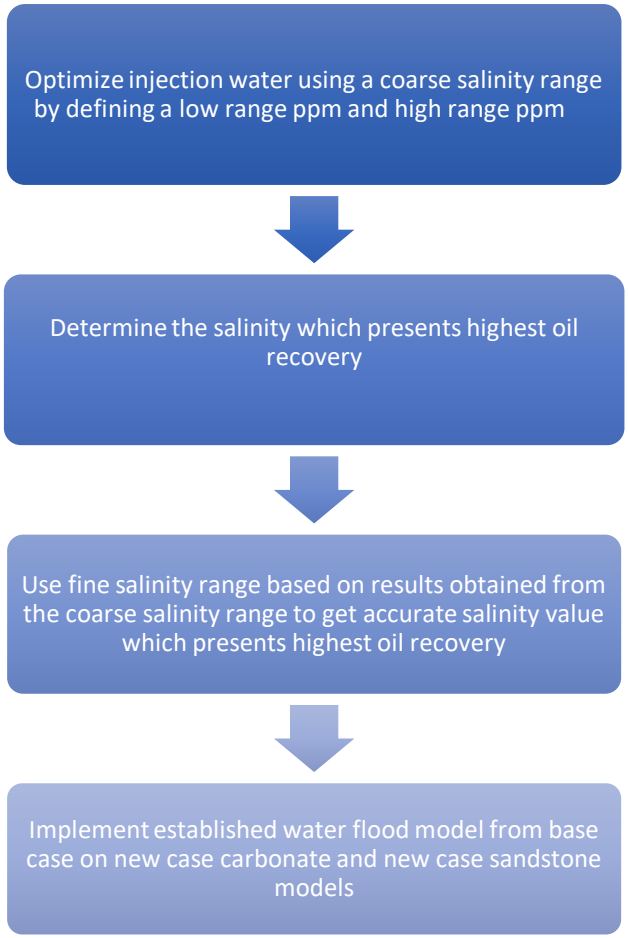

Figure 3.8: Optimization workflow of the injection water

3.5.1 Carbonate Core

The first step is to establish a validated waterflood model to simulate a new case scenario for the carbonate core. It will be used as a base case for comparing the different scenarios, and it will give an idea about the impact the different LSWF mechanisms have on oil recovery increase. The first step is to optimize the 40,000 ppm NaCl injection water and determine the

salinity of the NaCl that gives the highest oil recovery, which can be used for further analyses. This study will use the CMG-CMOST optimization and analysis tool, and it follows the statistical workflow summarized in Figure 3.8.

First, we implement a coarse range salinity optimization, using a high and low salinity range of 1,000 – 40,000 ppm and 40,000 – 80,000 ppm. This optimization process is run using the CMG-CMOST package, which is an optimization and analysis tool. The simulator will determine the optimum NaCl value that provides the highest oil recovery. The results of the coarse range optimization are summarized in Table 4.2. However, the coarse range salinity optimization results need further optimization to obtain a more accurate salinity. This is done by setting a fine salinity range based on the results obtained from optimizing the coarse salinity range. Results of the fine range salinity are also in Table 4.2.

After establishing the waterflooding model, the base case carbonate's injection and formation water salinities are now replaced with the formation water (FW) published by Lee et al. (2017) with a salinity of 26,958.1 ppm. The injection seawater published by CMG Tutorials (2018) has a salinity of 41,964 ppm. The compositions of both waters are shown in Table 3.5 and Table 3.7, respectively.

3.5.2 Sandstone Core

The same approach followed for the carbonate core is used here; the optimization workflow is shown in Figure 3.8. This optimization is based on the results obtained by Pouryousefy et al. (2016). The optimum brine injection water salinity was 2,000 ppm, with a recovery factor of 84.8% obtained after injecting 4 PVs. This optimization study was conducted to determine whether this salinity is the optimum value or not. The optimization will be divided into a coarse range salinity of 1,000 to 10,000 ppm and 10,000 to 30,000 ppm. To get more accurate results, a fine optimization study based on the optimum salinity of the coarse salinity results will be conducted with a 1,000 to 5,000 ppm salinity. Once the waterflood model is established, it will be implemented in the new case sandstone. Results are shown in Chapter 4.

3.6 Effect of Ions

The next step of the optimization study is to determine the effect of the most important potential determining ions (PDIs) on the oil recovery factor. This study will be conducted using the optimum salinity obtained from the previous section for the carbonate and sandstone cores. In this step, CMG-CMOST will be used as well. The impact of the $SO4^{-2}$ ions concentration on the oil recovery in carbonates is investigated because $SO4^{-2}$ are the divalent ions responsible for the ionic exchange (Akhmetgareev & Khisamov, 2015). In contrast, Na^{+}, $Ca^{2+,}$ and Mg^{2+}

ions are responsible for the ionic exchange in sandstone formations. However, based on the simulation and results of the Sobol analysis shown in Figure 4.17, Na^+ has the highest impact. Since the SO_4^{-2} and Na^+ ions [have] a high impact on the low salinity injection results, optimizing them and obtaining their critical value is important for carbonate rocks and sandstone rocks, respectively. The design of the simulation followed for this analysis is shown in Figure 3.9. The sensitivity analysis results to determine these divalent ions' impact on recovery are summarized in Chapter 4.

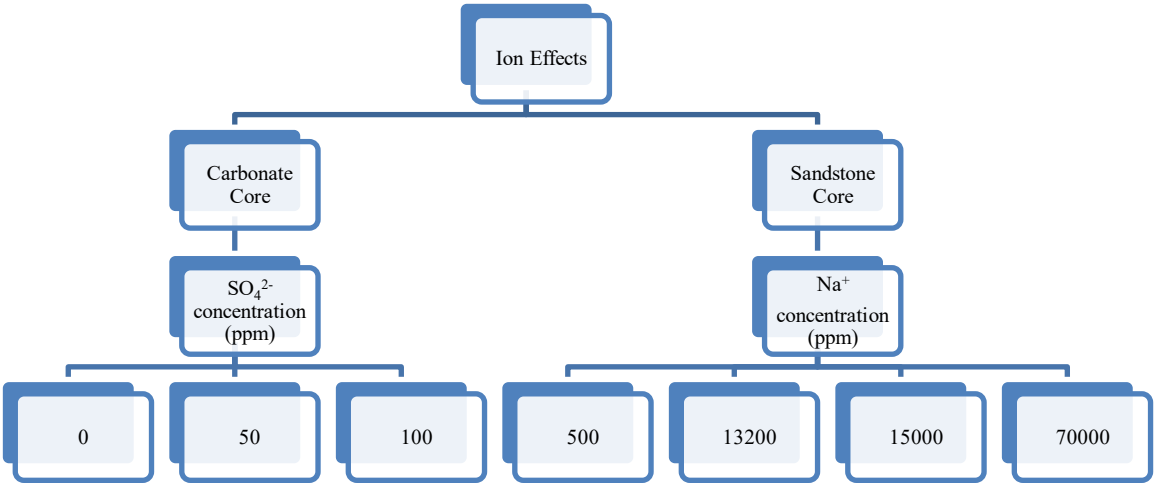

Figure 3.9: Flow chart of simulation runs for carbonate and sandstone cores

3.7 Investigation of Low salinity water flooding Mechanisms

Usually, injection water has a different mineral concentration than the formation water. Once injected, it disrupts the system's equilibrium, resulting in ion exchange and mineral dissolution/ precipitation, which are the low salinity water flooding (LSWF) mechanisms. Results and discussion of the mechanisms are shown in Chapter 4.

3.7.1 Mineral dissolution/ precipitation

To demonstrate the effects of LSWF on mineral dissolution and precipitation, the change in the moles of the minerals making up the rock is investigated from the inlet to the outlet. In CMG,

the sign convention for precipitation is (-ve) and (+ve) for dissolution. When these changes are significant, the rock's pore volume, porosity, and permeability are expected to change. The study of the aqueous component changes in the system from inlet and outlet can indicate the LSWF mechanism occurring in the system. Plots that show the impact of mineral dissolution/ precipitation on the pore volume, mineral mole change, and an aqueous component change are shown and discussed in Chapter 4.

3.7.2 Multi-ion exchange

By using CMG-GEM, multi-ion exchange (MIE), the LSWF mechanism can be magnified. The behavior of the effluent ions from the inlet to the outlet gives an idea about the interactions between the ions in the injection water with the rock's surface. Equations in Table 3.11 and Table 3.12 are used to activate this mechanism in the process wizard in CMG-GEM. Cation Exchange Capacity (CEC) is an important parameter that needs to be considered when investigating MIE's effects.

3.7.2.1 Cation Exchange Capacity (CEC)

The CEC is an intrinsic rock property that determines the maximum number of ions the rock surface can attract and absorb; above the maximum value of CEC, no more ions can be accepted. The higher the value of the CEC, the more ions can be absorbed onto the rock's surface. The ions that are originally attached to the rock's surface before any injection are exchangeable, meaning that once water is injected, it may be replaced. Rock types can be categorized based on their CEC value. The lower it is, the less advantage the rock has in terms of ion exchange. However, it should be noted that this does not correlate to a lower oil recovery factor. Na^+ can replace cations such as Ca^{2+} and Mg^{2+}. CEC works to influence the speed of the adsorption process; however, it doesn't have a major role in the amount of the Ca^{2+} saturation on the rock's surface (Pouryousefy, et al., 2016). The effect of using different CEC values is investigated by determining its impact on the Ca-X2 and oil recovery factor, and results are shown in Chapter 4.

3.8 Pilot-scale model

In this section, the core scale model is upscaled to a pilot-scale model to investigate the behavior of the LSWF in a five-spot two-layered pilot model by working with two cases: a homogeneous (using the same permeability and porosity as the core model) fractured reservoir and non-fractured reservoir. Random distribution of porosity and permeability is used to study the effect of heterogeneity on the fractured and non-fractured. The model's dimension was adopted from Kafry (2020), and they are shown in Table 3.13. For this pilot-scale model, one injection well

and four producers were designed in a five-spot model with an injection rate of 10 m^3/day using the injection water with ion composition summarized in Table 4.4 for the injection wells. Figure 3.10 shows the porosity and permeability in the homogenous model. Figure 3.11 shows the random distribution of the porosity and permeability in the heterogeneous model. New relative permeability curves representing the fracture system are shown in Figure 3.12 by implementing the Dual porosity- Dual permeability model.

Table 3.13: Pilot-scale model properties (Kafry, 2020)

Direction	I	J	K
Distance (m)	300	300	6
Cells	11	11	2
Porosity – Matrix	0.1	0.1	0.1
Porosity- Fracture	0.05	0.05	0.05
Permeability- Matrix (mD)	0.901	0.901	0.901
Permeability- Fracture (mD)	1000	1000	500
Fracture Spacing (m)	0.4	0.4	0.4

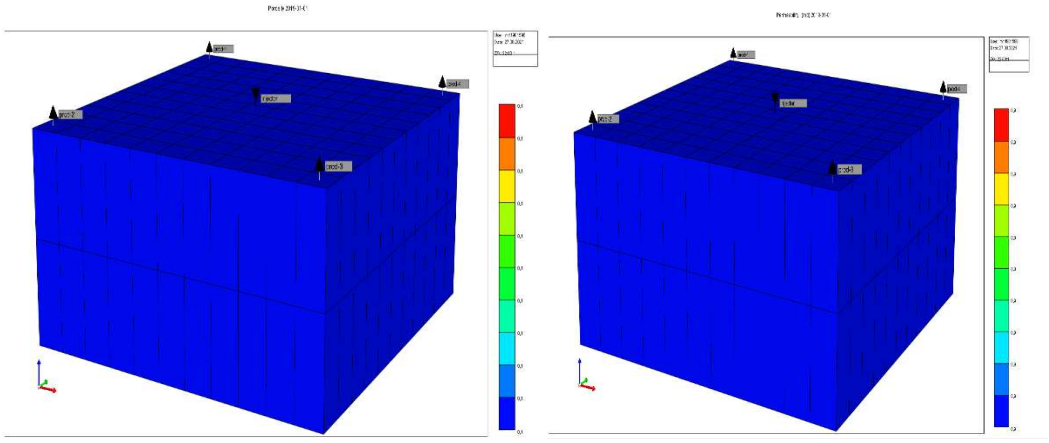

Figure 3.10: Porosity (left) and Permeability (right) in the homogeneous pilot scale model

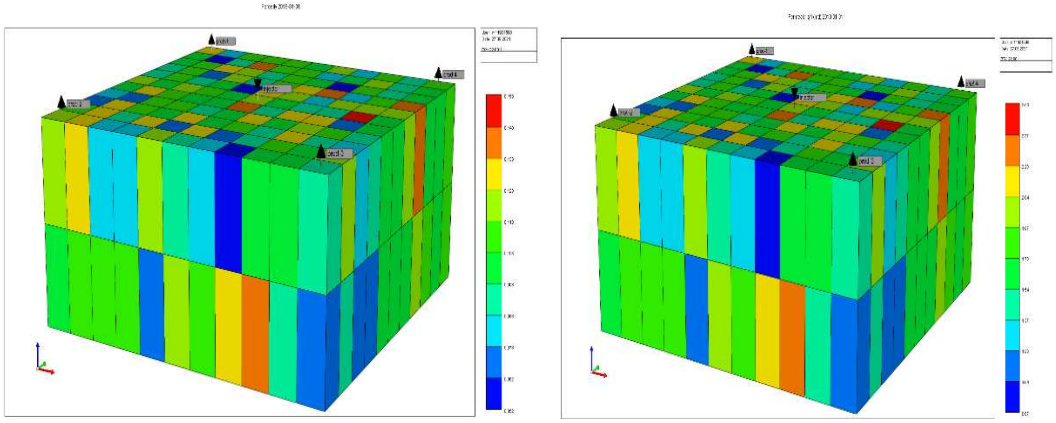

Figure 3.11: Random distribution of the Porosity (left) and Permeability (right) in the heterogeneous pilot scale model

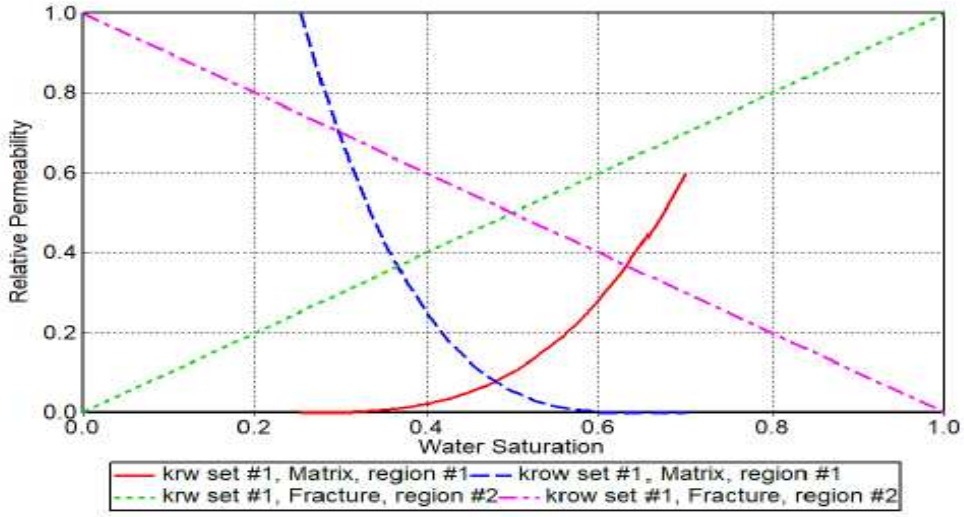

Figure 3.12: Relative permeability curves in the matrix and fractures for the pilot model

Chapter 4

Results and Discussion

The numerical modeling results obtained from the simulation runs are presented and discussed in the following sections.

4.1 Results Section

4.1.1 Water Optimization

The results of the water optimization for the carbonate and sandstone cores are discussed in the following section.

4.1.1.1 Carbonate Core

4.1.1.1.1 Optimization of Injection Water (base case carbonate)

Results of the coarse salinity range water optimization of the 40,000-ppm water are summarized in Table 4.1:

Table 4.1: Results of coarse salinity range optimization

Salinity Range (ppm)	Resulting Optimum Salinity (ppm)	Oil Recovery Factor (%)	Incremental increase from the initial case
1,000 - 40,000	5,223	56.8	17.8
40,000 - 80,000	43,750	47	8

Results of the water optimization are shown in Figure 4.1; when injecting 40,000 ppm NaCl water in the original case, a recovery factor of 38.9% was achieved. However, based on the results, 40,000 ppm NaCl water injection is not the optimum salinity for this formation. It is observed that the oil recovery increases by 17.8% from the original case as the NaCl

concentration decreases from 40,000 ppm to 5,223 ppm. Nevertheless, it cannot be considered the optimum and final water salinity composition because it used a coarse salinity range. The next step is to set a fine range to see the effect of smaller salinity ranges. The fine salinity range was set to be between 2,000 ppm and 8,000 ppm. This range was chosen based on the optimum salinity of NaCl from the coarse salinity range. The results of the optimization are summarized in Table 4.2. Figure 4.2 shows the results of the coarse range salinity for both 1,000 – 40,000 ppm and 40,000 – 80,000 ppm. Figure 4.3 shows the comparison between the coarse salinity ranges and base case, the lower coarse salinity range of 1,000-40,000 ppm gave a higher recovery. It will be used for the fine salinity range optimization.

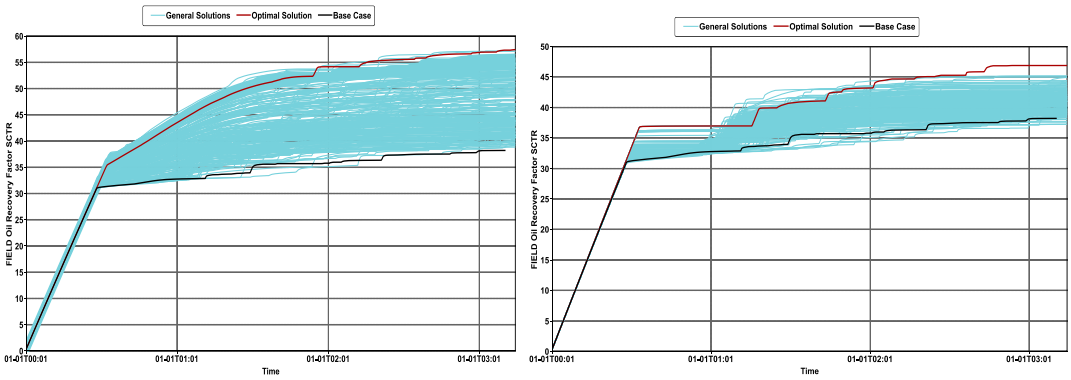

Figure 4.1: Coarse salinity range optimization: 1 - 40 K ppm (left) and 40 - 80 K ppm (right)

Table 4.2: Results of coarse and fine salinity range optimization of NaCl injection water

Salinity Range	Range (ppm)	Optimum Salinity (ppm)	Oil Recovery Factor (%)	Oil Recovery Increment from Base Case (%)
Coarse	1,000 – 40,000	5,223	56.8	17.8
Coarse	40,000 – 80,000	45,000	47	8
Fine	2,000 – 8000	3,911	58	19

Since the optimum coarse salinity of the brine was 5,223 ppm, a range between 1,000 to 6,000 ppm is used as the fine range salinity. It is shown that by using a finer salinity range, the results are higher in accuracy and present a higher oil recovery factor, leading to the conclusion that the highest oil recovery achieved is 58%, by injecting a brine of 3,911 ppm NaCl (Figure 4.3). The comparison between coarse, fine salinities with the base case is summarized in Table 4.2.

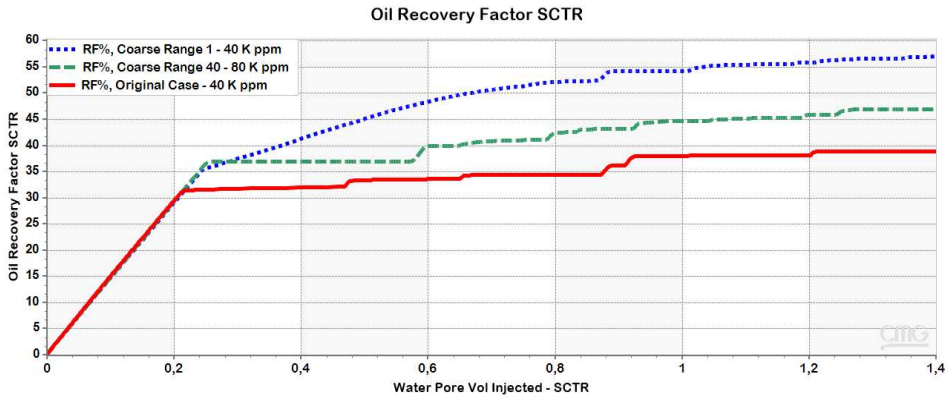

Figure 4.2: Recovery factor comparison between the two coarse salinities and base case

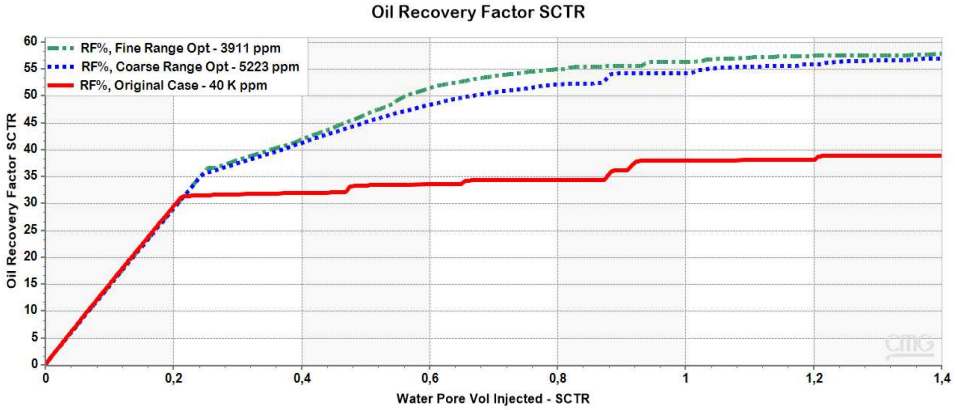

Figure 4.3: Recovery factor comparison between coarse, fine range salinities and base case

The reason for the incremental oil recovery during the reduction of the NaCl water salinity from 40,000 ppm to 3,911 ppm can be due to the ion concentration contrast, which causes a destabilization of the equilibrium state once existing in the rock-brine system, this results in wettability alteration resulting in an oil increment. However, in the high salinity injection water, it is difficult to determine the reason. It could be due to the high concentration of Na^+ in the injection water, which binds to the negatively charged carboxylic group forming Na+ - carboxylate component which is produced, reducing the oil in the reservoir and increasing the recovery.

4.1.1.1.2 Optimization of Seawater (new case carbonate)

The optimization steps for the new carbonate case will be adopted from the statistical approach done in the previous section shown in Figure 3.8. Seawater with the composition shown in Table 3.7 was used as the injection water, the brine in Table 3.5 is used as the formation brine

(FW) for the carbonate core. The coarse range salinity was set between 1,000 ppm – 40,000 ppm. CMOST generated several simulations to determine the salinity that gave the optimum results. As shown in Figure 4.4, the highest oil recovery was obtained with 4,396 ppm (blue curve) injection salinity; a recovery of 81.4% was obtained.

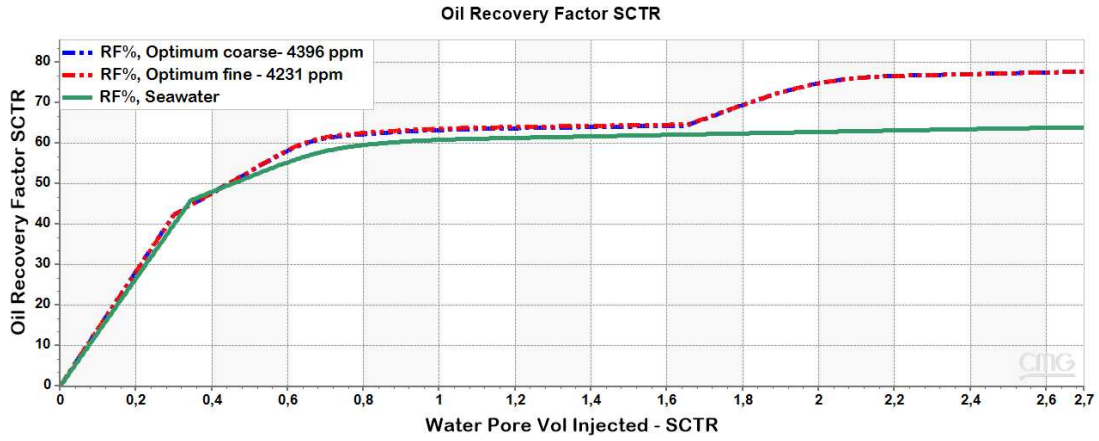

Figure 4.4: Optimization study of the Seawater (SW) using a coarse and fine salinity range

The salinity range has been reduced to be between 1,000 ppm and 6,000 ppm to get more accurate results. Simulation results show that the optimum salinity is not very far from the coarse salinity range. A salinity of 4,231 ppm gives a recovery factor of 81.5%, 0.01% higher than the coarse salinity range simulations. The coarse and fine salinity range optimization results are summarized in Table 4.3, and a comparison between the ion concentration of the initial seawater and optimized seawater is summarized in Table 4.4.

Table 4.3: Results of coarse and fine salinity range optimization for Seawater optimization

Salinity Range	Range (ppm)	Optimum Salinity (ppm)	Oil Recovery Factor (%)	Oil Recovery Increment from Base Case (%)
Coarse	1,000 – 40,000	4,396	81.4	17.7
Fine	1,000 – 6000	4,231	81.5	17.8

Table 4.4: Ion concentration comparison between initial and optimized seawater

	Ca^{2+} (ppm)	Mg^{2+} (ppm)	Na^{+} (ppm)	Cl^{-} (ppm)	HCO_3^{-} (ppm)	SO_4^{2-} (ppm)	Sum (ppm)
Initial Salinity of Seawater	511	1,540	13,200	23,400	163	3,150	41,964
Optimized Seawater	25.2	25.3	2610	1223	1.83	345	4,231

A comparison of the ions between the initial seawater and the optimized seawater is given in Table 4.4. As can be seen, the optimized seawater has a rather high concentration of monovalent ions (Na^{+} and Cl^{-}). These ions are non-active towards the carbonate rock stern layer. It means that they are present in the diffuse outer layer. These ions are preventing the other ions from reacting with the carbonate rock. However, when the Na^{+} is diluted five times and Cl^{-} 19 times, surface chemistry changes, allowing the PDIs to reach the carbonate rocks surface even at lower concentrations. As shown in Table 4.4, the SO_4^{2-} was diluted nine times, but recovery still increased.

The relative permeability curves of the high salinity and the optimum salinity are shown in Figure 4.5. It shows that by injecting the 4,231 ppm water into an oil/intermediate wet carbonate rock, the wettability of the rock will be altered to more water-wet conditions, which is evidence of the low salinity water effects.

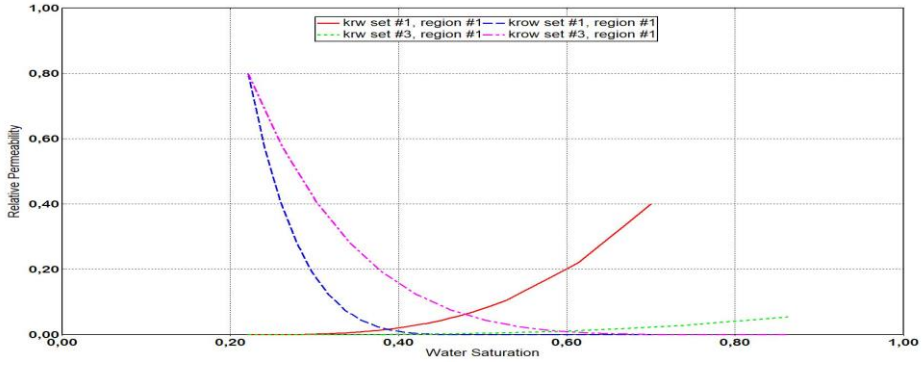

Figure 4.5: Relative Permeability in the carbonate rock for high salinity (blue/red) and low salinity (pink/green)

4.1.1.2 Sandstone Core

4.1.1.2.1 Optimization of Injection Water (base case sandstone)

The base case injection water scenario of the sandstone in this section is based on the work of Pouryousefy et al. (2016). The water has been optimized to determine whether the 10,000 ppm, which presented a recovery factor of 82%, is the optimum salinity, resulting in the highest oil recovery factor or not. By running the optimization simulation package offered by CMG-CMOST, the optimization of the water is possible. Like the carbonate core, two salinity ranges are used to optimize the water. First, a coarse salinity range of 1,000 to 30,000 ppm results showed that at a salinity of 1,362 ppm, the highest recovery factor of 86.2% was obtained. This is a 4.2% oil recovery increase from the original case.

However, to determine whether this is the optimum recovery or not, a finer (narrower) salinity range must be used based on the results of the coarser salinity. The salinity range was reduced to 1,000 to 5,000 ppm, based on the results. The optimum salinity was still 1,362 ppm. Results of base case sandstone are summarized in Table 4.5. Figure 4.6 shows the result of optimizing the NaCl by generating several runs in CMOST. Figure 4.7 shows the comparison in oil recovery factor between the base case and optimum NaCl case.

Table 4.5: Results of base case sandstone

	Salinity (ppm)	Oil Recovery Factor (%)	Oil Recovery Increment
NaCl only (Pouryousefy et al., 2016)	10,000	82	-
Base case sandstone	1,362	86.2	4.2

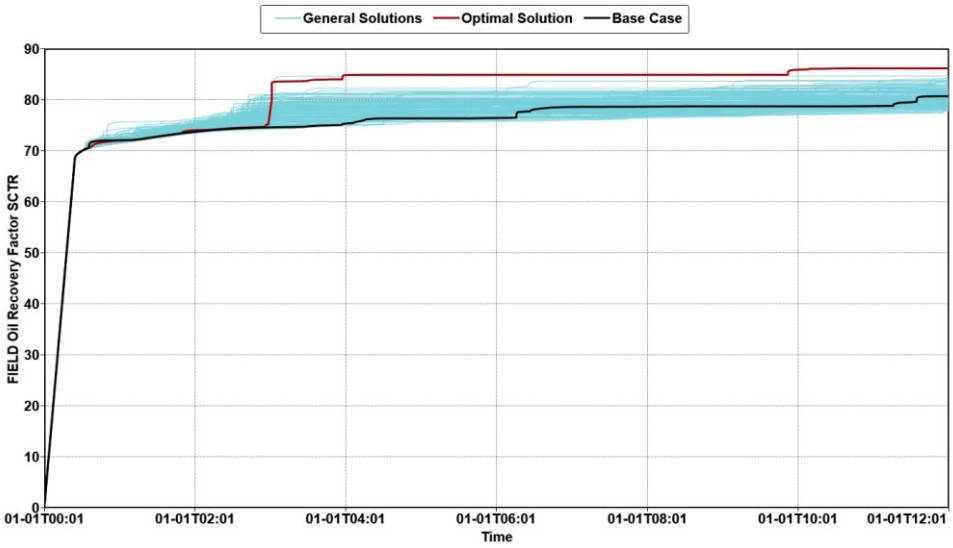

Figure 4.6: Optimization runs in the sandstone core with coarse range salinity using only NaCl water as injection water

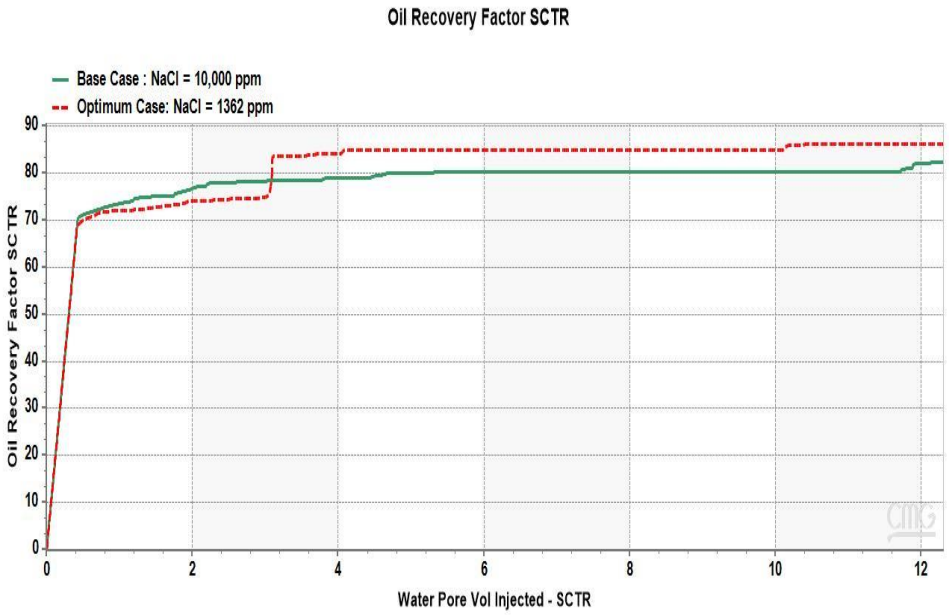

Figure 4.7: Results of optimization study of the NaCl only water using a coarse and fine salinity range compared to the base case

4.1.1.2.2 Optimization of Seawater (new case sandstone)

By running the optimization study on the seawater, the coarse and fine range of salinity results are shown in Table 4.6.

Table 4.6: Results of Seawater optimization

Salinity Range	Range (ppm)	Optimum Salinity (ppm)	Oil Recovery Factor (%)	Oil Recovery Increment from Base Case (%)
Coarse	5,000 – 50,000	7,670	88	13.4
Fine	5,000 – 8,000	7,670	88	13.4

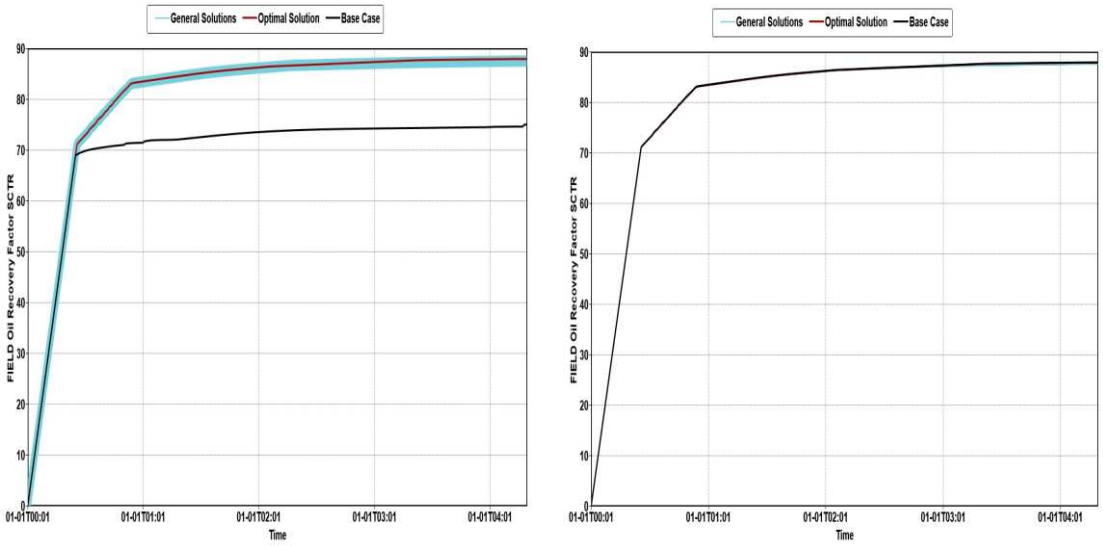

Figure 4.8: Results of the Coarse range salinity (left) and Fine range salinity (right)

Based on the results in Table 4.6. and Figure 4.8, the optimum salinity for the seawater in the sandstone core is 7,670 ppm. Reducing the salinity range to get more accurate results did not change the conclusion, as shown in Figure 4.8 (figure on the right). The optimum salinity (red curve) is identical to the base case curve (black), corresponding to the coarse salinity range. The results are shown in Table 4.7 and Figure 4.9.

Table 4.7: Comparison of the results of injecting different waters in sandstone core

	Salinity (ppm)	Oil Recovery Factor (%)	Oil Recovery Increment
Seawater (CMG Tutorials, 2018)	41,964	74.6	-
Optimized Seawater	7,670	88	13.4

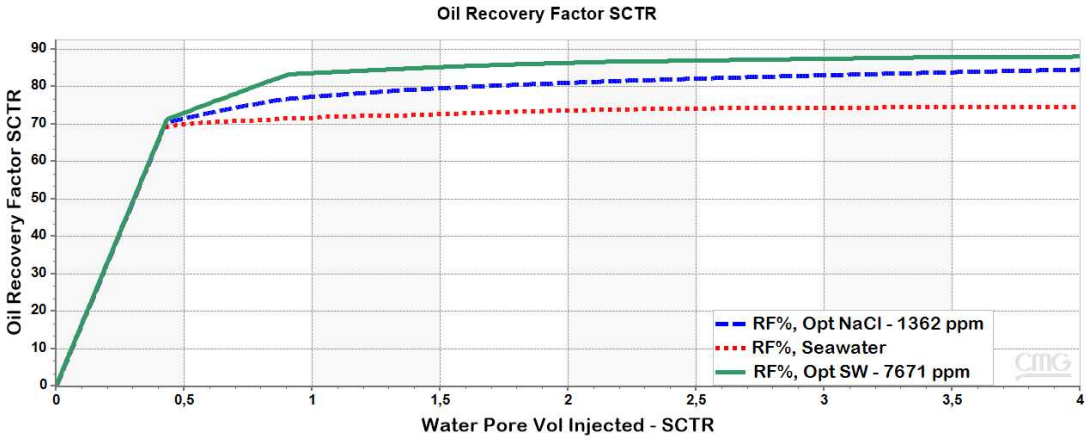

Figure 4.9: Results of optimization study of Seawater (CMG Tutorials, 2018) using a coarse and fine salinity range compared to the base case and NaCl – 1,362 ppm

From the previous results, it can be concluded that the seawater can be optimized to present higher results, and at a salinity of 7,670 ppm, it recovered a total of 88% oil. A comparison between the composition of the original and optimized seawater is shown in Table 4.8. The main reason for the oil recovery increment is the reduction of the cations that bind between the negatively charged oil and sandstone surface. During low salinity water injection in the sandstone core, the ionic water concentration is poorer in cations. The Ca^{2+} ion was diluted 36.5 times, Mg^{2+} 19 times, and Na^{+} was diluted 3 times. This results in increased repulsive forces between the clay and oil as they are both negatively charged, and less divalent ions bind both negatively charged surfaces. This causes the double layer's expansion, resulting in the increased distance between the clay surface and absorbed oil, causing the oil desorption from the clay surface.

Table 4.8: Comparison between the composition of the initial and optimized seawater for the new case sandstone

	Ca^{2+} (ppm)	Mg^{2+} (ppm)	Na^{+} (ppm)	Cl^{-} (ppm)	HCO_3^{-} (ppm)	SO_4^{2-} (ppm)	Sum (ppm)
Initial Salinity of Seawater	511	1,540	13,200	23,400	163	3,150	41,964
Optimized Seawater	14	78.6	4,152	3,057	2.9	365	7,670

4.1.1.3 Pilot-scale model

This section investigates the results of injecting the optimized seawater into a carbonate pilot scale model. The composition of the optimized seawater is summarized in Table 4.4. The pilot-scale model is a five-spot model created for the homogeneous and heterogeneous fractured and non-fractured models. The recovery factor for the non-fractured homogeneous is shown in Figure 4.10. It shows no big difference between the heterogeneous and homogeneous systems when injecting the optimized seawater into the two cases. The homogeneous system recovered a total of 83%, whereas the heterogeneous system recovered 85%. In this case, the heterogeneity of the reservoir had a positive effect on oil recovery.

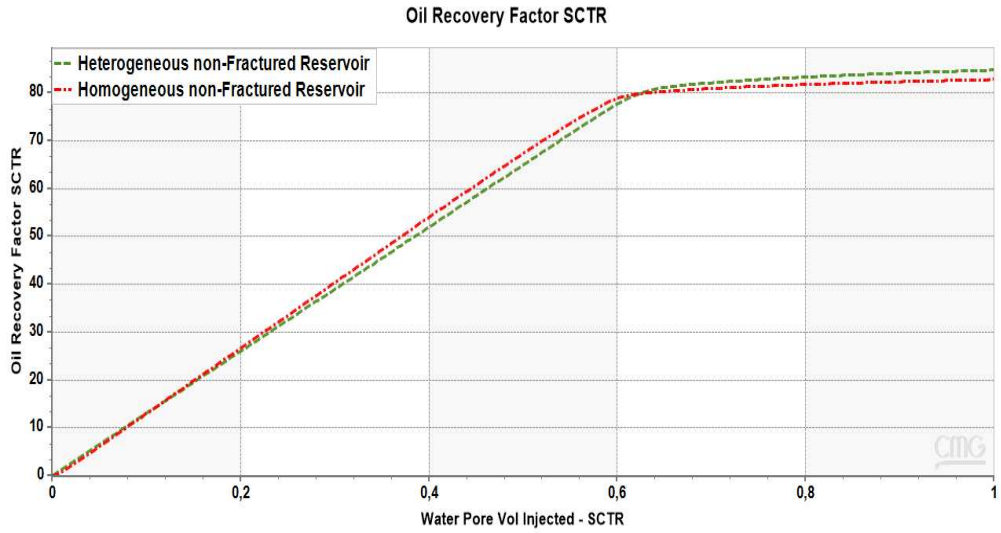

Figure 4.10: Pilot model oil recovery factor in the non-fractured reservoirs

A lower recovery factor was observed in the fractured reservoir for homogeneous and heterogeneous systems, as shown in Figure 4.11. The fractured homogenous reservoir recovered a total of 82.7%, whereas the heterogenous reservoir recovered 76.5%. The 6.2% less recovery in the heterogeneous reservoir is due to the random distribution of properties, meaning that heterogeneity had a negative effect in this case. The heterogeneous non-fractured reservoir recovered 8.4 % more than the fractured cases. This is because fractures can positively or negatively impact the fluid flow and hence oil recovery.

Fractured networks in a reservoir can sometimes cause the uneven sweeping of the reservoir, resulting in an early breakthrough of the injection fluid and a lower recovery. The breakthrough occurred in the fractured reservoir earlier than the non-fractured reservoir (Figure 4.10 and Figure 4.11). The reason for this earlier breakthrough of the fractured reservoir can be due to high water mobility in the fracture channels, which results in uneven sweeping in the reservoir.

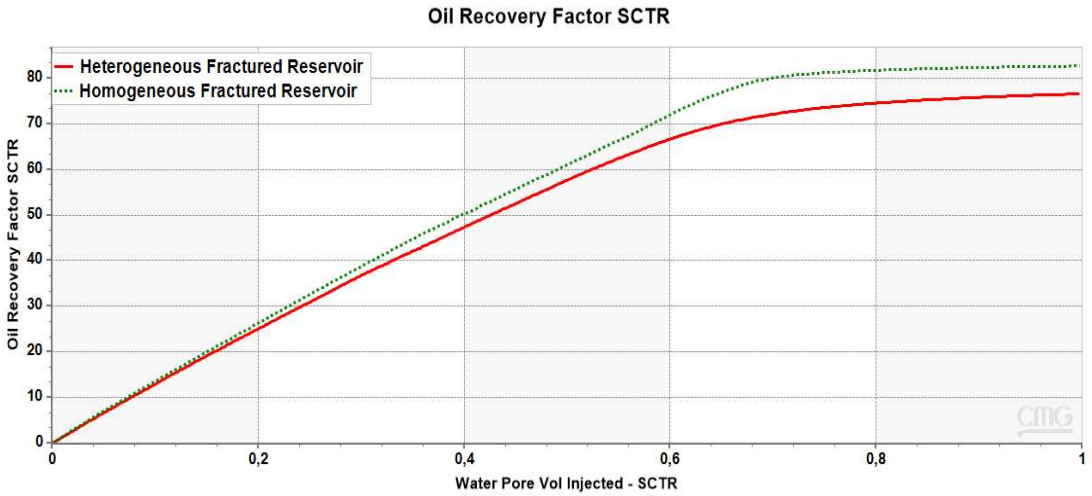

Figure 4.11: Pilot model oil recovery factor in the fractured reservoirs

Figure 4.12 and Figure 4.13 show a section of the reservoir before and at the breakthrough time of the heterogeneous fractured reservoir. It shows that water breakthroughs in the producer wells for the heterogeneous case before the homogeneous case.

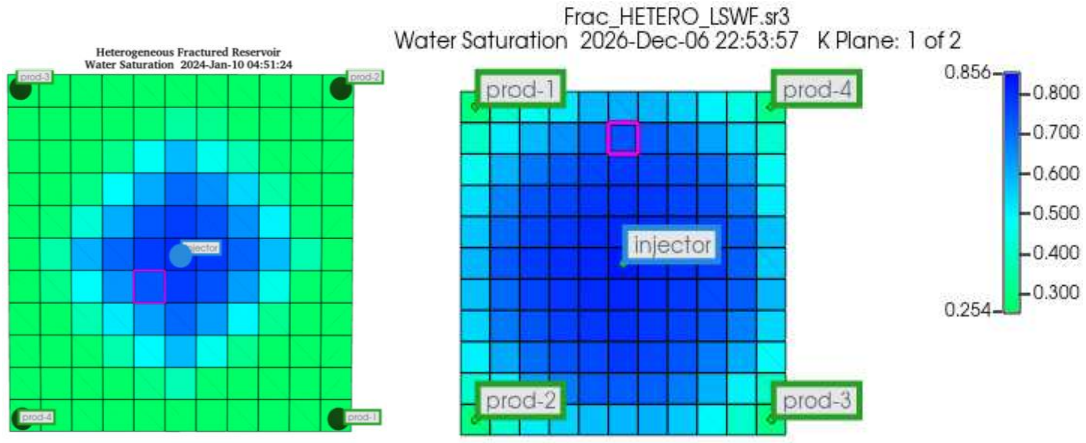

Figure 4.12: Depiction of water saturation movement in Heterogeneous reservoir from before water breakthrough (left) to at water breakthrough (right)

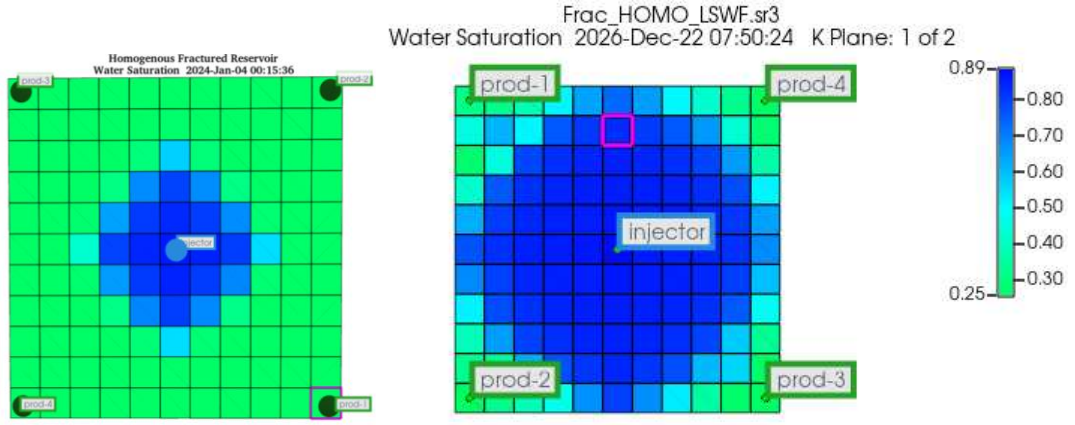

Figure 4.13: Depiction of water saturation movement in Homogeneous reservoir from before water breakthrough (left) and at breakthrough time of Heterogeneous reservoir (right)

The oil recovery factor obtained for the non-fractured reservoir is 83%, whereas for the fractured reservoir its 82.57 %, which is only a 0.43 % increment from the non-fractured case. This means that the fractures don't significantly impact the oil recovery factor since both cases have almost the same recovery factor. The breakthrough in the fractured reservoir occurred slightly before the non-fractured reservoir. Results of the recovery factors for both heterogeneous and homogeneous reservoirs are shown in Table 4.9.

Table 4.9: Oil recovery factors for pilot-scale model

	Oil Recovery Factor (%)	
Reservoir Type	Fractured	Non-Fractured
Heterogeneous	76.6	84.8
Homogeneous	82.57	83

Table 4.9 shows that a lower recovery factor was obtained for the heterogeneous reservoir for the fractured system. This is due to assuming a heterogeneous system, which is usually the case in carbonate rocks. Another reason is that the LSWF injection water movement in the reservoir is uniform in the homogeneous system. The injection water will reach all the pores in the rock and contact the highest specific area of the pores compared to the heterogeneous reservoir. However, the injection water will move at a different velocity in the heterogeneous reservoir depending on the pore distribution. Some pores may be plugged, preventing the injection water from reaching the entire pore system.

4.1.2 Effect of Ions

The ion concentration of SO_4^{2-} for the water injected into the carbonate core and Na^+ for the water injected into the sandstone core will be altered to determine the impact of the ion concentration on the oil recovery and mineral dissolution/ precipitation. In carbonates, the presence of SO_4^{2-} as the divalent ions are responsible for the ion exchange process. In sandstone cores, the Na^+ and other divalent ions such as Ca^{2+} and Mg^{2+}, linked to the polar compounds in the crude oil and sandstone surface, are responsible for causing the repulsive forces that expand the double layer.

The simulation runs presented in the following sections are designed to understand the divalent ions' impact on both cores to increase recovery, summarized in Figure 3.9.

4.1.2.1 Carbonate Core

CMG-MOST uses the Sobol analysis (variance-based sensitivity) to determine the effect of different ions on the ultimate recovery factor. Sobol analysis determines the important ion concentration of the injection water concerning recovery. Based on the Sobol analysis, SO_4^{-2} has the highest impact on the oil recovery factor for the carbonate core, as shown in Figure 4.14.

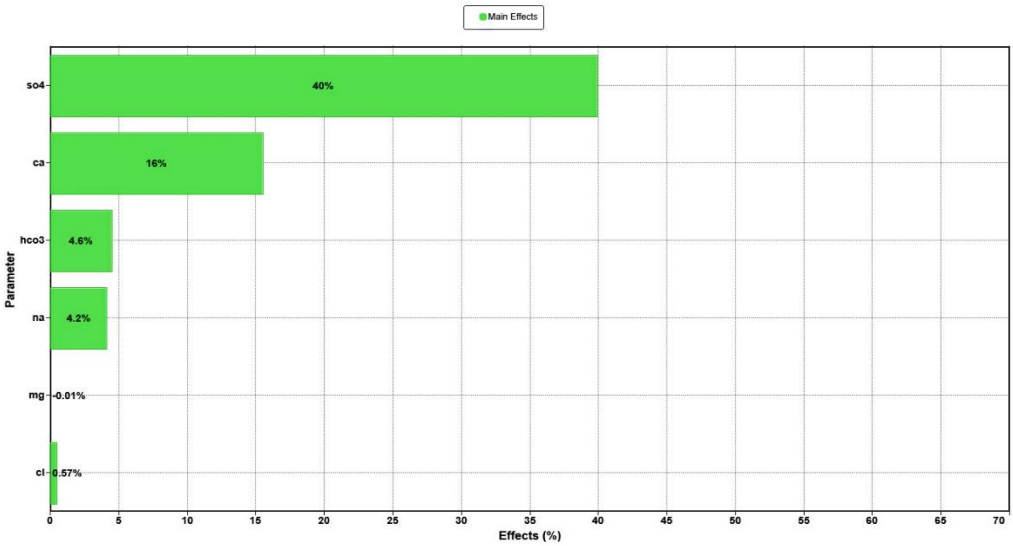

Figure 4.14: Sobol Analysis on ion effects impact on the oi recovery in the carbonate rock

To understand the impact of SO_4^{2-} in carbonate cores, sensitivity analysis using CMG-CMOST will be utilized using a composition of the injected water of 3,911 ppm (NaCl only) obtained from the water optimization study conducted in the base case carbonate. After injecting 1.4 PVs of water into a carbonate core, Figure 4.15 shows the impact of injecting three different $SO4^{-2}$ values, which are 100 ppm, 50 ppm, and the original case, which has 0 ppm of SO_4^{-2}. The results in the Figure show that increasing the $SO4^{-2}$ concentration from 0 ppm to 50 ppm resulted in an oil recovery increase from 36.4% to 70.5%. The bar chart shown in Figure 4.16 confirms a critical concentration of SO_4^{-2} in carbonate rocks, above or below which oil recovery will be lower.

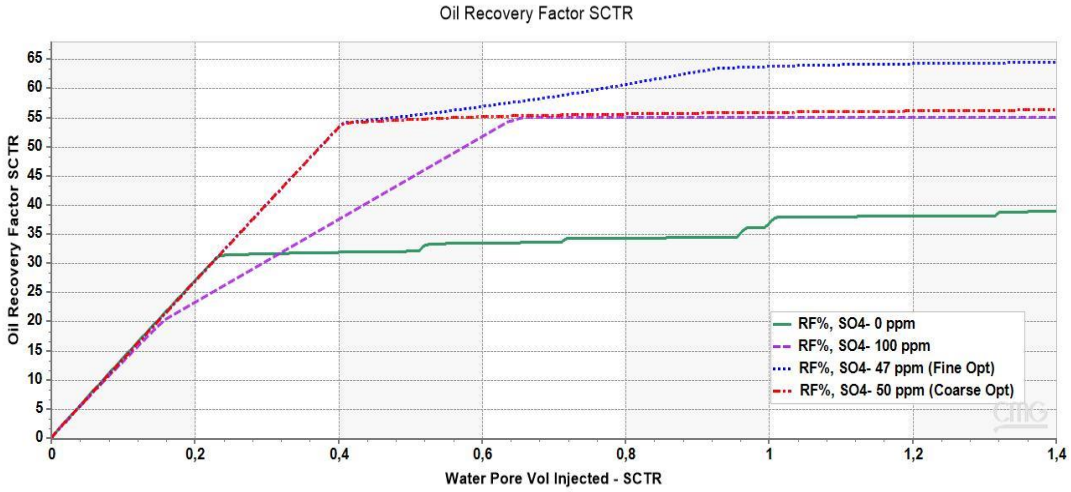

Figure 4.15: SO_4^{-2} effect on Oil Recovery for a carbonate core after injecting 1.4 PVs of NaCl water

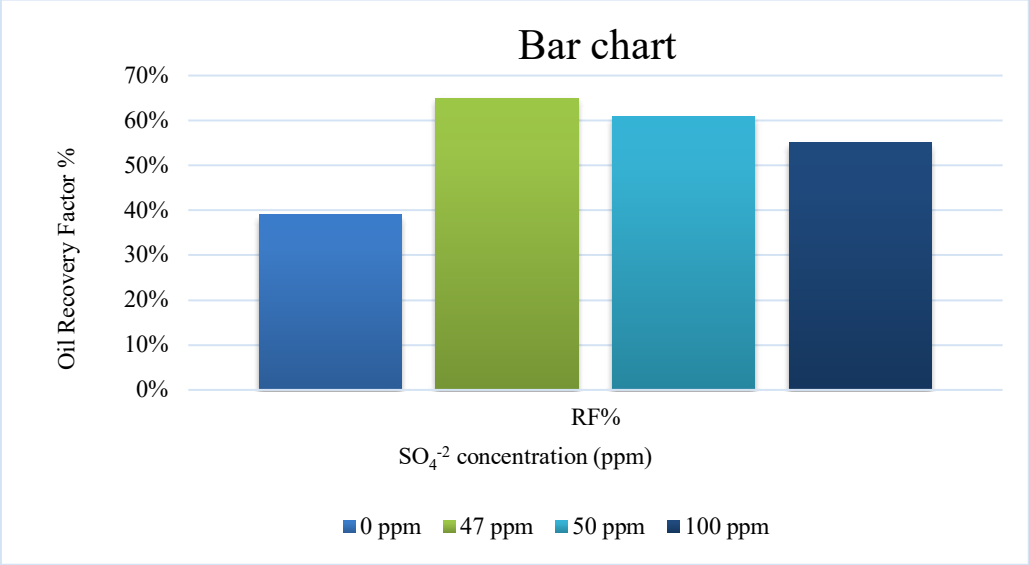

Figure 4.16: Bar chart of oil recovery difference by varying SO_4^{-2} values for a carbonate core after injection 1.4 PVs of NaCl water

As it is clear from the results in Figure 4.15 and Figure 4.16, the variation of recovery factor with SO_4^{-2} is not following the same trend. The recovery factor increased when the concentration of SO_4^{-2} increased from 0 ppm to 47 ppm. This is because as the SO_4^{-2} concentration increases, the oil produced increases as well. However, it decreased from 47 ppm to 100 ppm. This was because, at 47 ppm, the rock's surface will be saturated with SO_4^{-2} ions. The ion exchange process will not occur anymore because no oil is attached to the rock surface; hence, no oil recovery increase will be noticed. The optimization study showed that the critical SO_4^{-2} concentration is 50 ppm. However, another optimization study was conducted to determine the exact critical concentration of SO_4^{-2}. At a concentration of 47 ppm and a recovery factor of 65%, a 26% incremental oil was achieved from the base case.

4.1.2.2 Sandstone Core

The impact of the Na^+ ion is studied for the sandstone core. It has the highest impact on the oil recovery based on the Sobol analysis (Figure 4.17). The analysis used the following Na^+ ion concentrations: 500, 13,200 (concentration of Na^+ in initial seawater), 15,000, and 70,000 ppm. The results show that reducing the Na^+ concentration from 13,200 ppm to 500 ppm gave an incremental oil recovery of 12.7 %. The oil recovery factor increased as the Na^+ ions concentration decreased, as shown in Figures 4.18 and 4.19. However, decreasing the Na^+ concentration below 500 ppm did not show any further increase in oil recovery, making 500 ppm of Na^+ ions the critical value as shown in the bar chart in Figure 4.19. No further increase

was observed because no further Na^+ ions will be attached to the rock's surface, which means no further ion exchange between the rock and the injection water is expected.

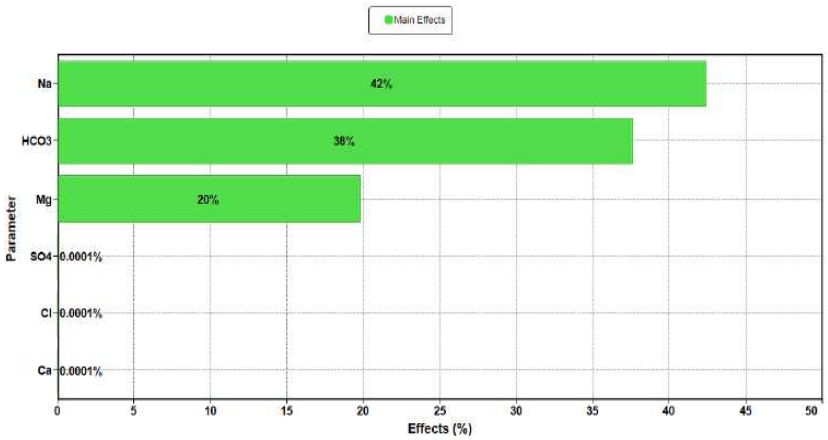

Figure 4.17: Sobol Analysis on ion impact on the oil recovery in the sandstone rock

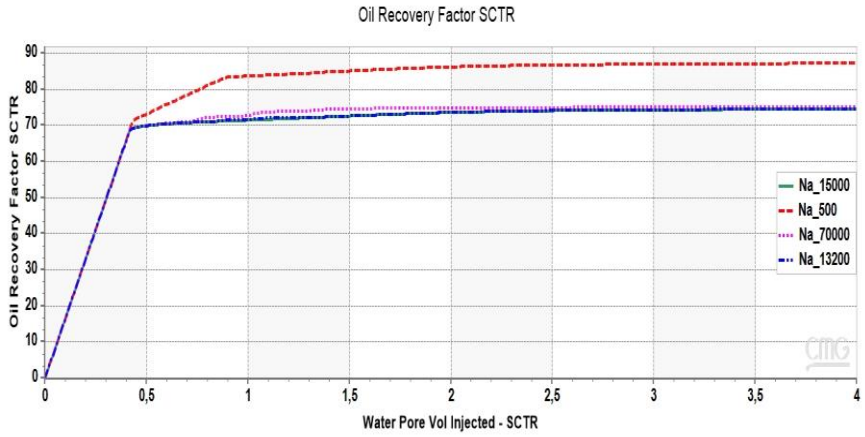

Figure 4.18: Na^+ effect on Oil Recovery for a sandstone core after injecting 4 PVs of NaCl water

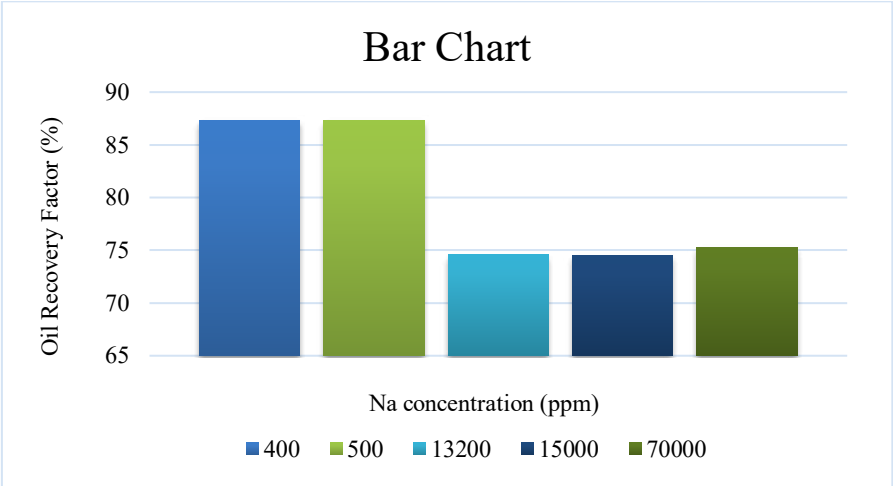

Figure 4.19: Bar chart of oil recovery difference by varying Na^+ ion values for a sandstone core after injecting 4 PVs of Seawater

4.1.3 Investigation of LSWF mechanisms

Results and discussion of the effect of the LSWF mechanisms for carbonates and sandstones are shown below:

4.1.3.1 Effect of mineral dissolution/ precipitation

4.1.3.1.1 Carbonate Core

In this section, the optimized seawater with compositions shown in Table 4.4 was injected into a carbonate rock with formation water shown in Table 3.5. Both waters have different ionic compositions, so it is expected that a disruption in the system will occur, such as ion exchange and mineral dissolution/precipitation.

The carbonate core comprises 50% calcite and 50% dolomite. Figure 4.20 shows the effect of injecting LSWF on the minerals. In CMG, the negative sign is the evidence of mineral precipitation, whereas the positive sign is evidence of mineral dissolution. Calcite dissolved while not much change occurred to the dolomite, which means that the LSWF has a higher effect on the calcite than the dolomite. Even though this effect is not that significant could be due to the small length scale and time of the process.

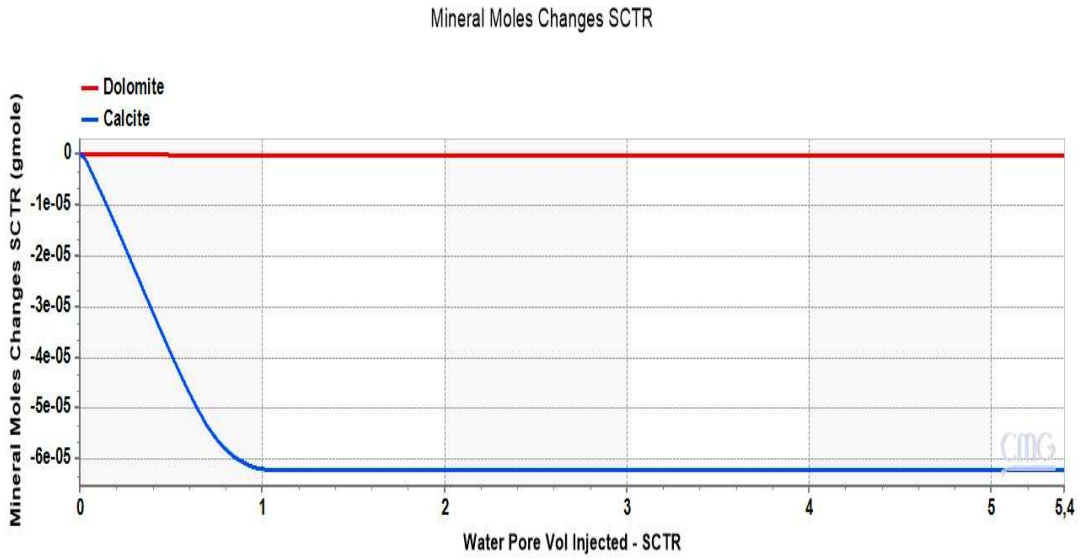

Figure 4.20: Mineral Mole change for ions in formation water for carbonate core

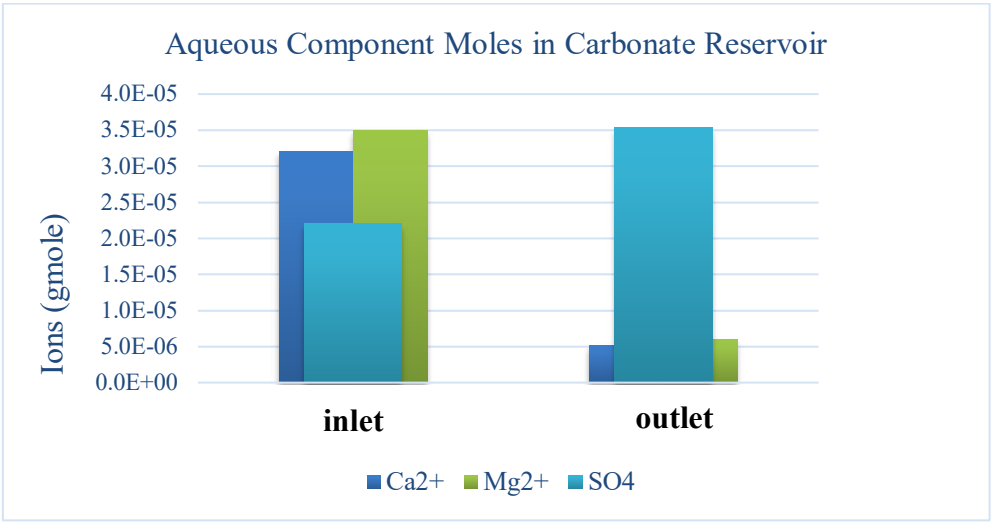

Figure 4.21: Aqueous Component changes in the carbonate core

As shown in Figure 4.21, the ion concentration of Ca^{2+}, $SO_4^{-2,}$ and Mg^{2+} changes from the inlet (where it's at formation water conditions) to the outlet (where the optimized seawater had already been injected). It shows that the concentration of the divalent ions (Ca^{2+}, Mg^{2+}) reduced as the optimized seawater was injected. However, the concentration of the SO_4^{-2} increased from the initial to the final time step. The concentration of SO_4^{-2} in the injection water was almost similar to the formation water.

Figure 4.22 shows that the mineral dissolution in the core was not very significant after 5.4 PVI. The increase in the pore volume was less than 0.11 %. This insignificant change in the pore volume of the carbonate core after LSWF could be due to the small length and time scale in which the reactions have not had the significant time to react with the minerals in the core. However, based on analyzing the effluent ion composition in Figure 4.21, a reduction in Ca^{2+} production is evidence of mineral precipitation.

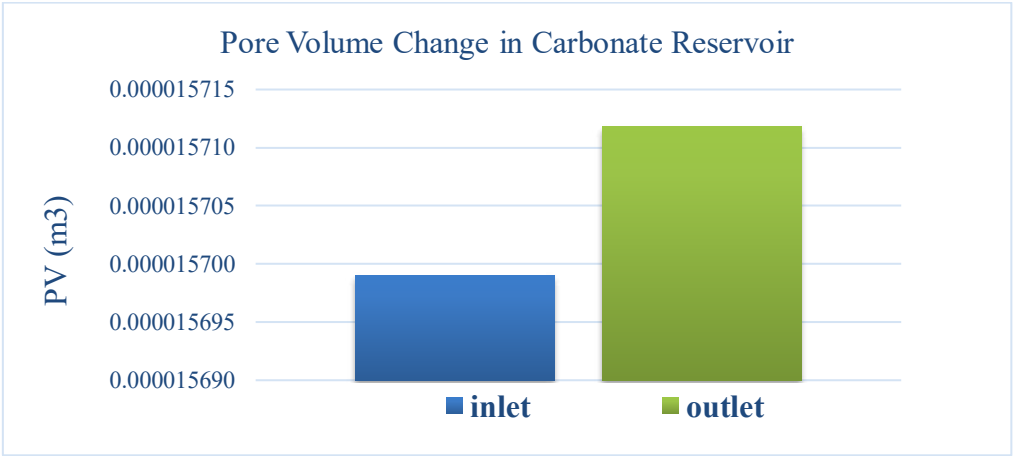

Figure 4.22: Pore volume change in the carbonate core after 5.4 PVI

4.1.3.1.2 Sandstone Core

Figure 4.23 shows the effect of LSWF on the minerals in the formation, calcite and feldspar are dissolving, and the other minerals such as quartz and the clays (illite and kaolinite) are precipitating.

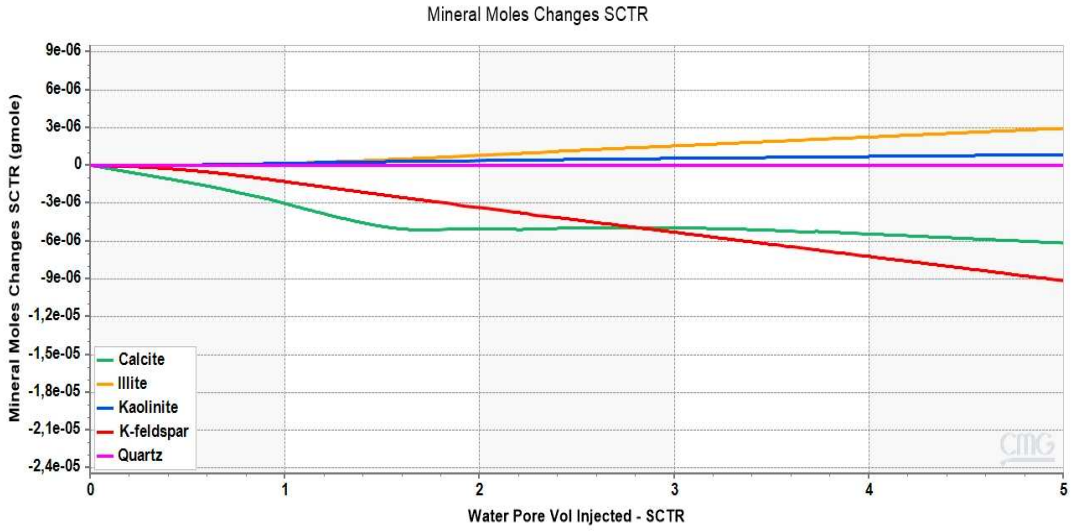

Figure 4.23: Mineral Mole change for ions in formation water for sandstone core

Figure 4.24 shows the change in the aqueous components in the sandstone core. The Na^+ ions concentration in the injection water is less than the formation, so that the outlet value will be less. Nevertheless, a slight change in the concentration of the Ca^{2+} and Mg^{2+} from inlet to outlet is observed. Though, the slight increase in the Ca^{2+} production is evidence of mineral dissolution.

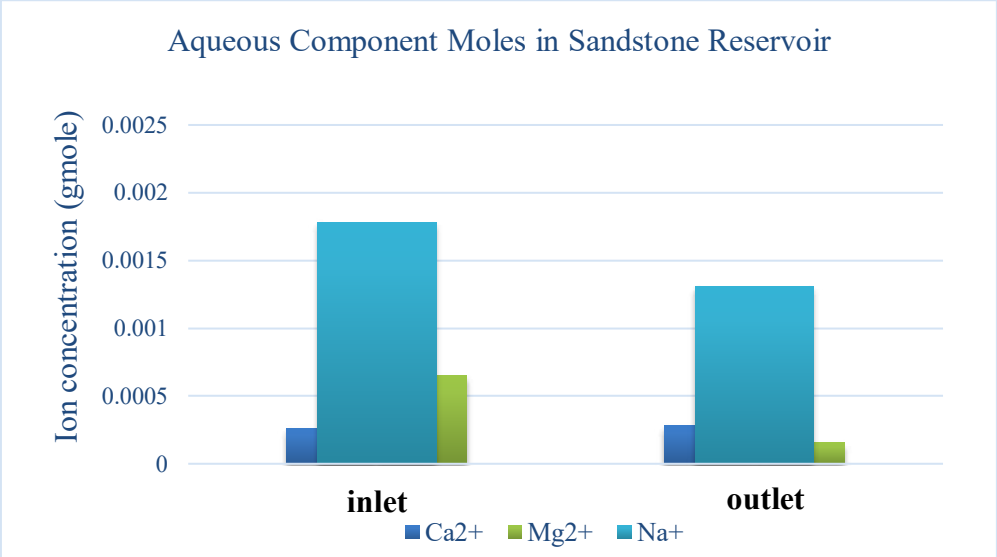

Figure 4.24: Aqueous Component changes in the sandstone core

Like the carbonate case, the change in pore volume, as shown in Figure 4.25, is negligible, meaning that the mineral precipitation/ dissolution is not having any significant impact on the porosity or permeability in the core scale model. This may be due to the little time of the process.

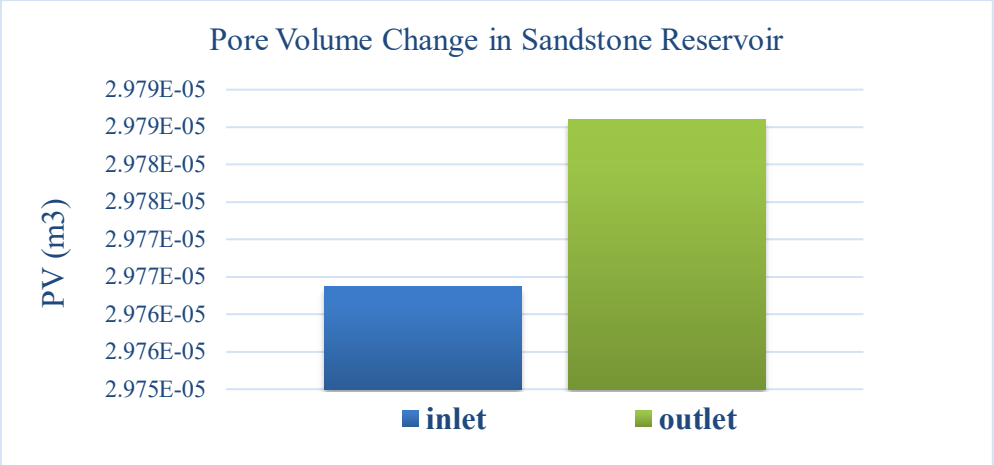

Figure 4.25: Pore volume change in the sandstone core

4.1.3.1.3 Pilot-scale model

Figure 4.26 and Figure 4.27 depict the aqueous component change from the inlet to outlet in the non-fractured and fractured homogeneous reservoirs. The results of ions shown in the five-spot model are different than that of the core scale model. For the non-fractured homogeneous reservoir, the Ca^{2+} and Mg^{2+} ions increase from inlet to outlet, whereas the SO_4^{-2} reduces. This increase in Ca^{2+} and Mg^{2+} can be due to the dissolution of the ions. The decrease of the SO_4^{-2} is because during the LSWF, the repulsive effect between the charged surfaces increases. The double-layer is expanding, resulting in the replacement of the absorbed crude oil with SO_4^{-2} ion. It causes a reduction in the rock's surface charge. This causes an electrical repulsion and release of the attached oil. This results in the adsorption of the SO_4^{-2} ion and desorption of the absorbed crude oil, hence increasing the recovery.

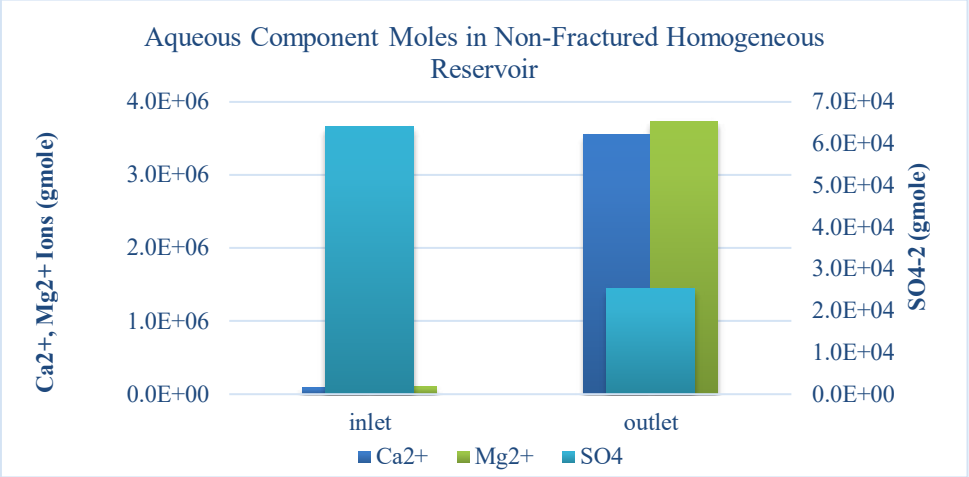

Figure 4.26: Aqueous component change during LSWF in the non-fractured homogeneous reservoir

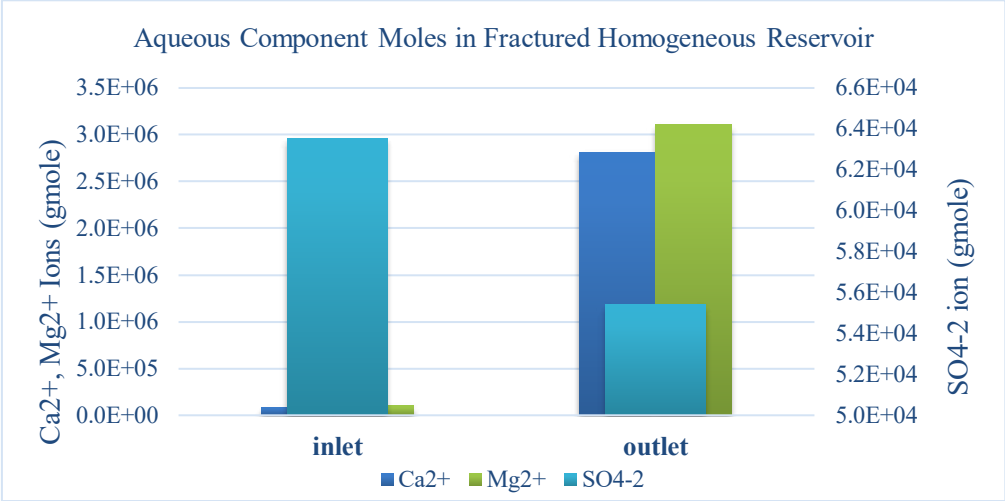

Figure 4.27: Aqueous component change during LSWF in the fractured homogeneous reservoir

Figure 4.28 shows the dissolution of the minerals in the rock. This dissolution effect is confirmed in Figure 4.29. It shows that the pore volume in the non- fractured reservoir increased from the inlet to the outlet.

Figure 4.28: Mineral precipitation in the non-fractured homogeneous reservoir

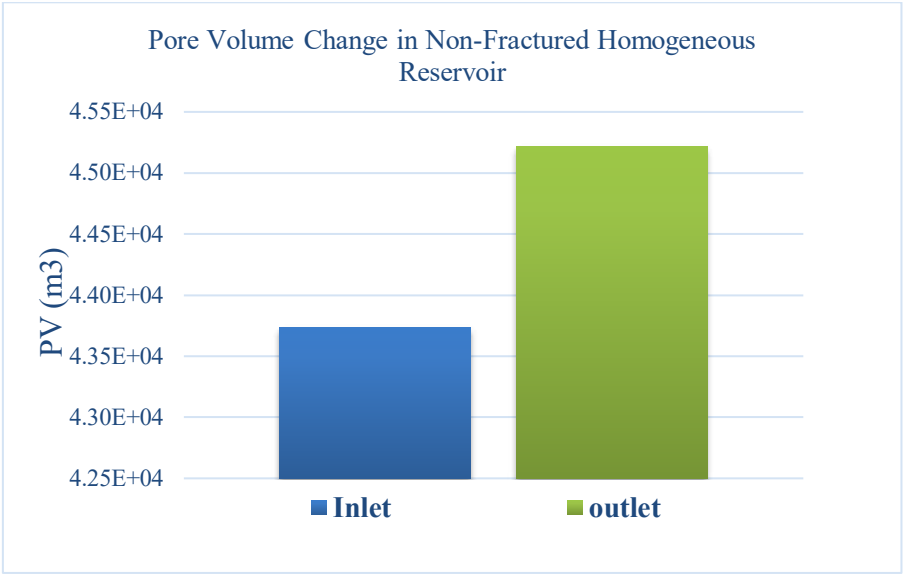

Figure 4.29: Pore volume change from inlet to outlet in the non-fractured homogeneous reservoir

The fluids will contact less surface areas in the fractured homogeneous reservoir because some fractures could be sealed, diverting the flow to the open fractures only. This will result in lower mineral dissolution than the non-fractured case. Figure 4.30 shows the effect of mineral dissolution in the fractured homogeneous reservoir, which increases the pore volume, as shown in Figure 4.31.

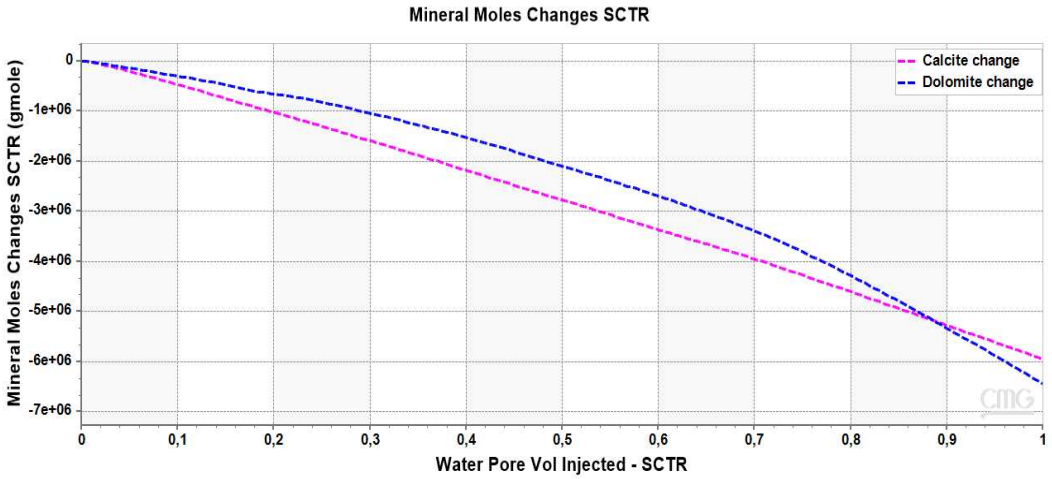

Figure 4.30: Mineral Dissolution in the fractured homogeneous reservoir

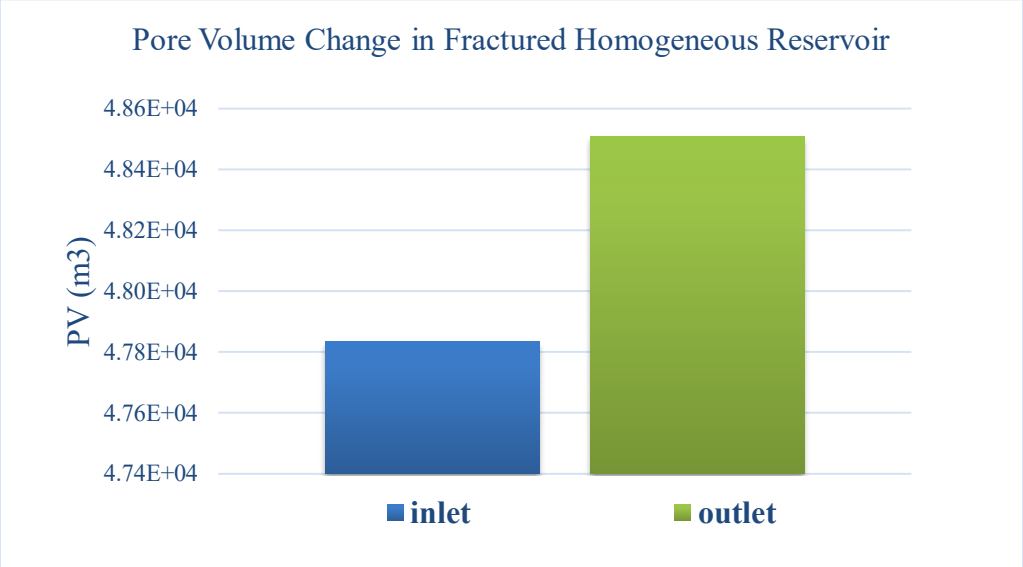

Figure 4.31: Pore volume change from inlet to outlet in the fractured homogeneous reservoir

Mineral dissolution/ precipitation change in the matrix and fractures of the homogeneous fractured system are shown in Table 4.10. A very small reduction in the pore volume of the matrix system is seen making it. However, a 17 % increase in the pore volume of the fracture system is seen. This could be because the water flows into the fractures and imbibes into the matrix. This causes the LSWF reactions to be more active in the fractures than in the matrix system. Resulting in the pore volume change occurring mostly in the fracture system.

Table 4.10: Pore Volume change in fracture and matrix system

	Pore Volume (m3)		
System	Inlet	Outlet	Increase (%)
Matrices	4,35E+04	4,32E+04	-0.69
Fractures	4,52E+03	5,27E+03	17

4.1.3.2 Effect of multi-ion exchange

In this section, LSWF simulations were conducted using the multiple ion-exchange mechanisms (MIE) for sandstone and carbonated by activating Equation 3.18 and Equation 3.19. The results of the activation of this LSWF mechanism are shown next.

4.1.3.2.1 Carbonate Core

As MIE is highly dependent on the composition of the formation and injection water, the formation water of the rock must contain specific ions named the PDIs. The potential determining ions are Ca^{2+}, $Mg^{2+,}$ and Na^{+}. Due to the work of MIE, the divalent ions (Ca^{2+}, Mg^{2+}) attached to the rock's surface will be replaced by ions such as Na^{+} from the injection water during the LSWF. This will result in the desorption of the oil from the rock, leading to an oil recovery improvement.

The geochemical reactions were simulated by injecting the optimized seawater. Results in Figure 4.32 show that the Na^{+} concentration drops fast and becomes constant at around 0.4 PVI. However, the Ca^{2+} concentration was very low and dropped to zero immediately because the Ca^{2+} concentration in the formation water is around 12 times the amount in the injection water. If the concentration of the divalent ions in the injection water is higher than their concentration in the formation water, there would be an increased molality of the divalent ions, and spontaneous adsorption occurs, which results in the full saturation of the ion exchange site by those ions.

Figure 4.33 shows that the Ca-X2 increases initially where the calcite is being dissolved to compensate for the reduction in the Ca^{2+} ions. It reached equilibrium at around 2.1 PV, and then the Ca-X2 will start to reduce. Basically, the higher the adsorption of the Ca^{2+} ion on the carbonate core, the lower the recovery will be (MIE theory).

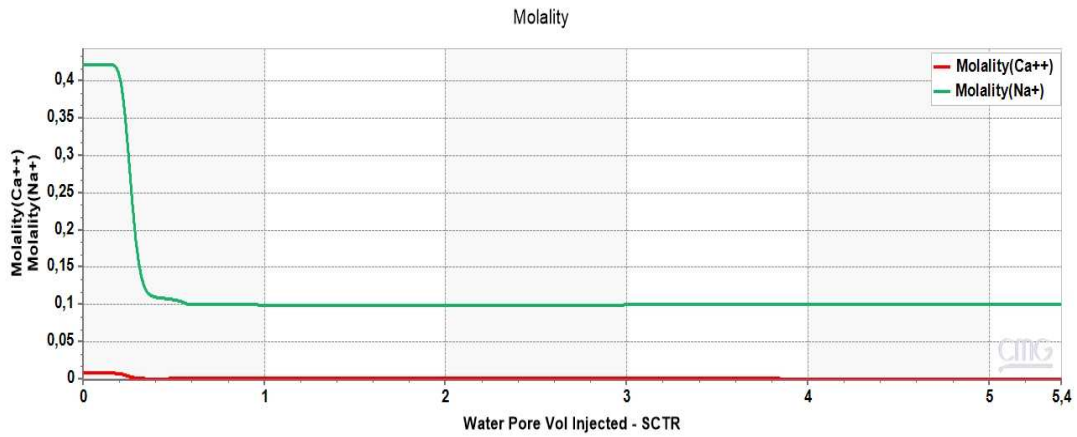

Figure 4.32: Cation concentration during injecting 4,230 ppm optimized seawater in carbonate core

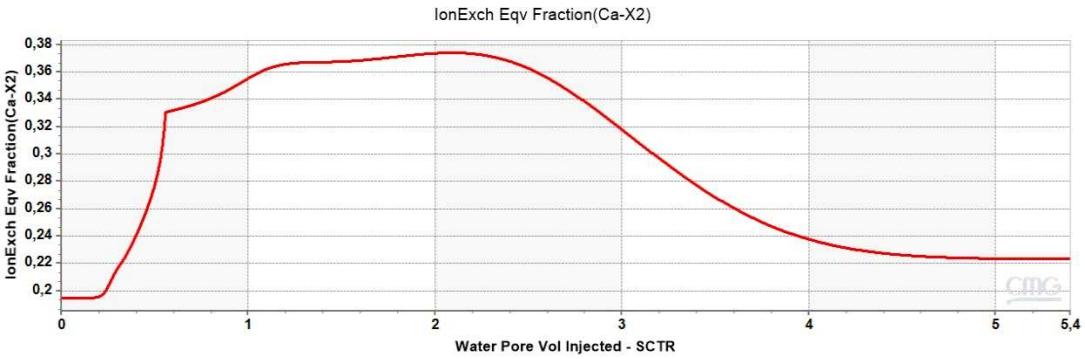

Figure 4.33: Adsorption of the divalent cations during injecting 4,230 ppm optimized seawater in carbonate core

4.1.3.2.2 Sandstone Core

The variation of the PDIs in the system can explain the MIE process in the sandstone rock. The interaction between the Na^{+}, $Ca^{2+,}$ and the rock interface during mineral dissolution and precipitation is studied. The equivalent fraction of Ca^{2+} on the reservoir rock (Ca-X2) is considered.

First, the sandstone rock's optimum NaCl only case (NaCl– 1,362 ppm) is simulated. The variation in concentration of Na^{+} and Ca^{2+} after injecting seven pore volumes is shown in Figure 4.34.

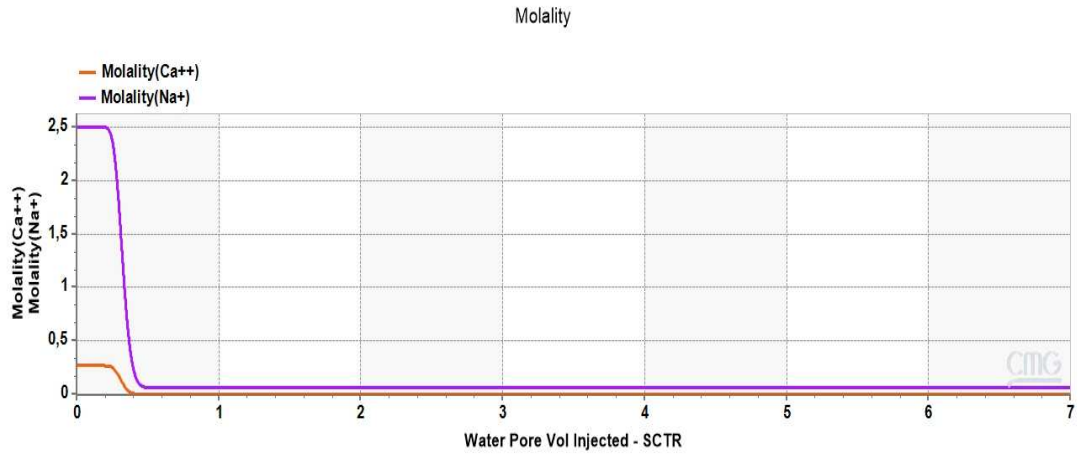

Figure 4.34: Cation concentration during 1362 ppm NaCl injection

As shown in Figure 4.34, the concentration of Na^+ decreased dramatically from its initial value. This is due to the lower concentration of Na^+ in the injection water than in the formation water, which causes a reduction of the Na^+ molality in the system. The figure also observes that the molality of Ca^{2+} decreases to zero, and this is because only NaCl water is being injected. The concentration of Ca^{2+} in this injection water is zero. Based on the MIE theory, the higher the concentration of the Na^+ ions compared to the Ca^{2+} ions, the more the Na^+ ions will adsorb onto the rock's surface. The desorbed oil components will accompany the Ca^{2+} ions. This occurs even though the Ca^{2+} has a higher affinity towards the rock surface than the Na^+ ions.

Figure 4.35 describes the amount of Ca^{2+} ion absorbed onto the rock surface. In the beginning, as the water pore volume injected is increasing, there's an increase in the amount of Ca^{2+} being absorbed onto the rock's surface. This is due to the dissolution of the calcite in the formation, which results from the decrease of Ca^{2+} ions in the system. The calcite dissolution compensates for the reduction of Ca^{2+} ions due to a disruption in the thermodynamics of the system caused by injecting a solution with a different salinity than the formation salinity.

However, once the thermodynamics of the system stabilizes, the Ca-X2 starts to decrease, as shown at around 2.5 PVs, and the Ca^{2+} ions are being desorbed from the rock. In contrast, the Na^+ ions are being absorbed according to the MIE theory. Basically, the higher the amount of Na^+ ions being absorbed to the surface in comparison to the desorption of the Ca^{2+} ions, the less the Ca^{2+} ions can create a bridge between the rock and oil, which leads to desorption of oil and oil recovery increase.

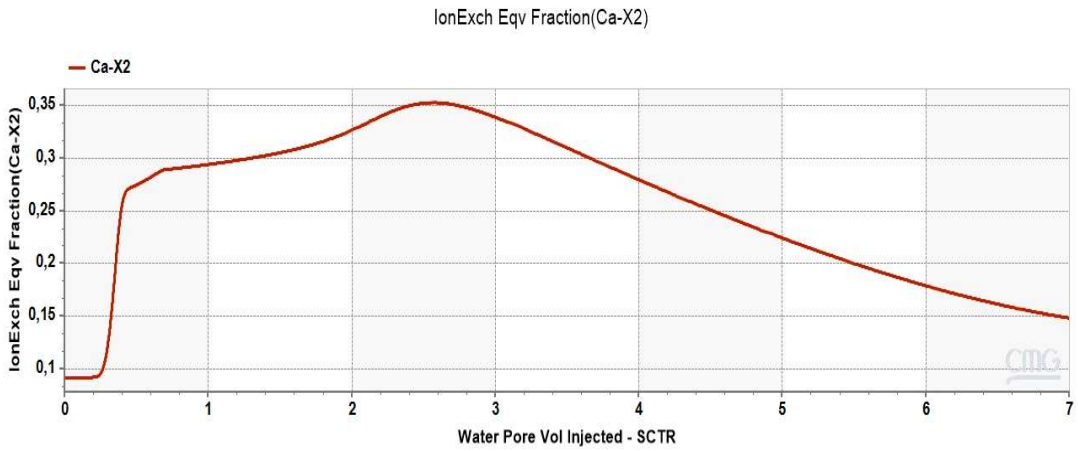

Figure 4.35: Adsorption of Ca^{2+} cation during 1,362 ppm NaCl injection

The same process was conducted for the new case sandstone, using the optimized seawater salinity (7,670 ppm). Figure 4.36 shows the molality for both ions (Na^{+} and Ca^{2+}). A similar trend as the first case is observed. In this case, the concentration of both cations is less than what is originally present in the formation water.

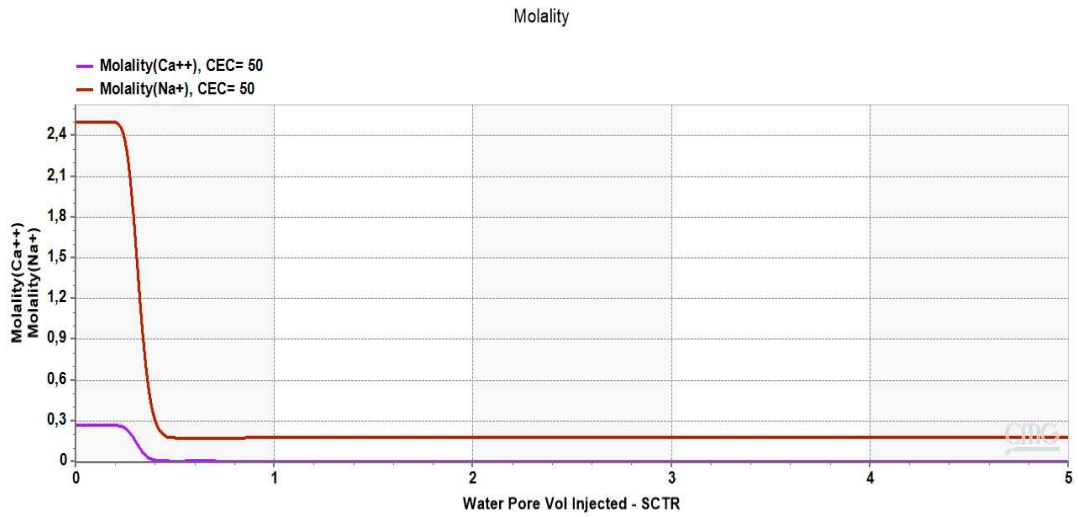

Figure 4.36: Cation concentration during 1,362 ppm NaCl injection

Figure 4.37 shows the response of adsorption of Ca^{2+} ions on the rock surface during the injection of the optimized seawater. Like the previous case, initially, there's an increase of Ca^{2+} ions adsorption on the rock. This is because in the system, due to the MIE, the Ca^{2+} concentration is reducing, as shown in Figure 4.36, so to compensate for this reduction, calcite is dissolving. However, unlike the previous case, it reached equilibrium much faster at around 0.7 PVs. As most of the Ca-X2 has been substituted with the Na^{+} ion, high recovery is expected as the ability of the Ca^{2+} to form a bridge between the rock and crude oil is lost.

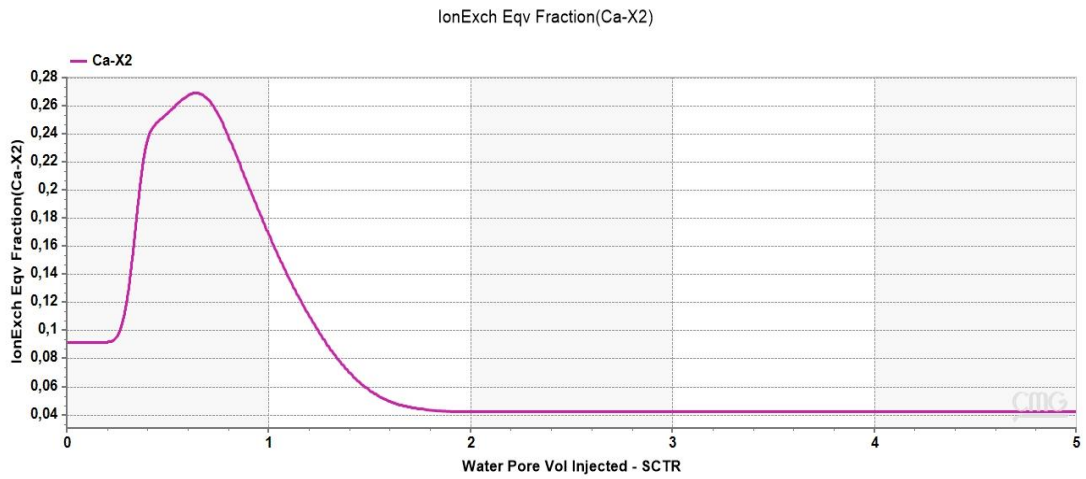

Figure 4.37: Adsorption of Ca^{2+} cation during 7,670 ppm NaCl injection

4.1.3.2.3 Cation exchange capacity (CEC)

Figure 4.38 shows the results of simulating three different CEC values equivalent to 50, 100, and 150. The investigation focused on correlating the effect of CEC on the number of absorbed/desorbed cations with the oil recovery factor. Figure 4.39 shows that CEC – 50 the system was faster in reaching equilibrium, and the calcite was dissolved quicker to compensate for the Ca^{2+} ion decrease. The literature suggests that clay minerals with a higher CEC effectively increase the recovery, but this isn't the case for kaolinites. They have a smaller CEC and still can have a high recovery. However, as the CEC increased in this study, it took much more time to reach equilibrium and the calcite dissolved slower as there was much more space on the rock surface for cation absorption.

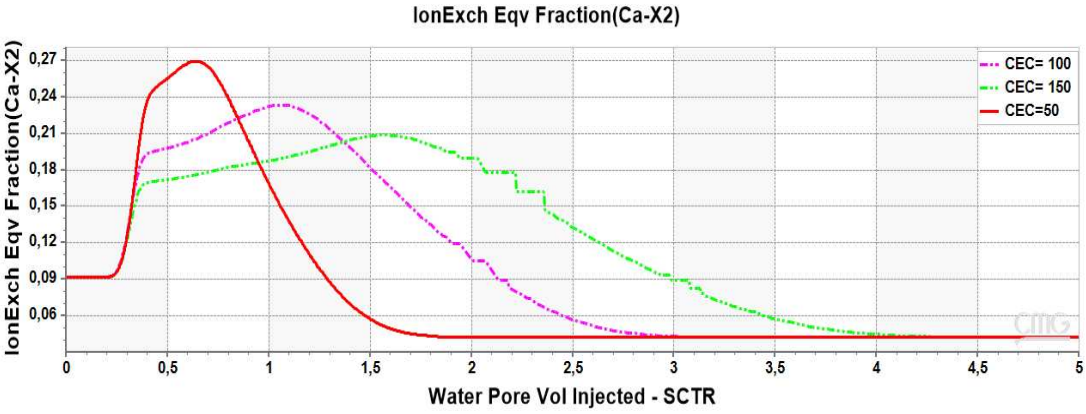

Figure 4.38: Effect of CEC on the adsorption of the Ca^{2+} ions on the sandstone rock during injection 7,670 ppm water

Based on Figure 4.39, the highest oil recovery was obtained at CEC – 50. The CEC affects the surface potential, impacting the repulsion forces between negatively charged clay and crude oil, resulting in oil higher recovery.

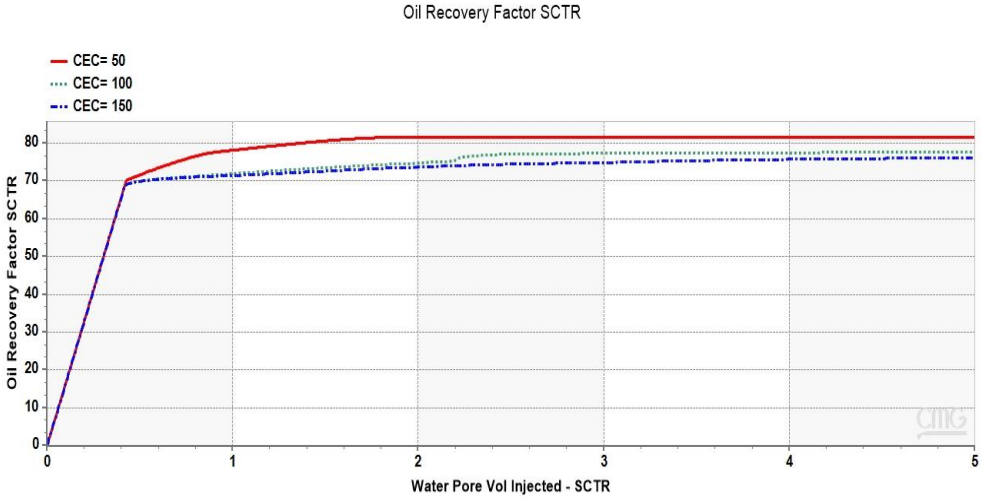

Figure 4.39: Effect of CEC on the oil recovery factor of the sandstone rock with clay during injection 7670 ppm water

When the clay (kaolinite and illite) content was reduced from 5.8 wt % to zero (no clay), the influence of CEC on the recovery factor is shown in Figure 4.40. CEC didn't influence the recovery, and the recovery factor for the three runs was almost identical; the results are shown in Table 4.11. It is not a big difference from when clay was present because the content of clay in the first case was only 5.8 wt %. However, a difference of 4.2% in recovery is seen when the CEC is at a value of 50, which is optimum when the clay is present. As shown in Figure 4.39, CEC impacts the recovery in the presence of clay and shows that a CEC of 50 gives the highest recovery (results shown in Table 4.11).

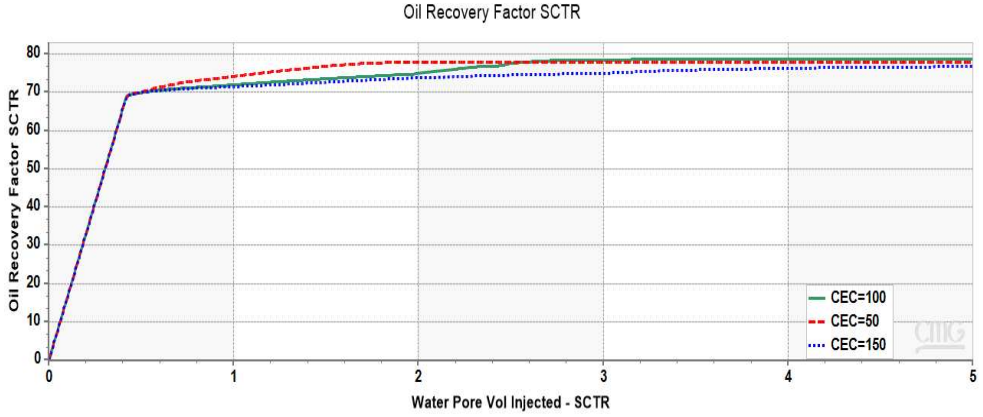

Figure 4.40: Effect of CEC on the oil recovery factor of the sandstone rock with no clay during injection 7670 ppm water

Table 4.11: Comparison of the impact of CEC on recovery for sandstone with and without clay

	Oil Recovery Factor (%)	
CEC	Clay	No Clay
50	82	77.8
100	78.2	78.2
150	77.2	76.7

4.1.4 Mineral Impact

The following section discusses the impact of LSWF using different mineral compositions for sandstone and carbonate rocks.

4.1.4.1 Mineral effect in Carbonates

The optimized seawater with composition summarized in Table 4.4 is injected into the carbonate core with composition in Table 4.12 to see the effect of LSWF using carbonate cores with different mineral compositions; the three cases are shown in Table 4.12. The results showed the highest recovery factor when the carbonate rock was made from equal amounts of calcite and dolomite (Case 1). The high dolomite case presented a higher recovery than the high calcite case. The difference in recovery between case 2 and case 3 is not that noticeable. This could be due to the higher amount of Mg^{2+} in the rock formation reacting with the injection water and causing the double layer to expand during the multi-ion exchange.

Table 4.12: Cases used to investigate the effect of LSWF on different mineral compositions

Case	Calcite	Dolomite	Recovery Factor (%)
Case 1	50%	50%	81.5
Case 2: High Calcite	80%	20%	58.9
Case 3: High Dolomite	20%	80%	60.7

4.1.4.2 Mineral effect in Sandstones

Two cases have been conducted to investigate the clay's impact on the recovery factor, as shown in Table 4.13; the case in which clay was present in the sandstone mineralogy presented a

13.3 % higher recovery than when it was absent (results shown in Table 4.13). The higher recovery might be due to the higher amount of ions in the clay mineralogy that impact the multi-ion exchange. This leading to the double layer expansion. In conclusion, it can be said that clay content in the sandstone core affects the oil recovery factor.

Table 4.13: Clay effect on recovery in sandstone core

Case	Clay percentage (wt%)	Recovery factor (%)
Case 1: Clay present	5.8	88
Case 2: Clay neglected	0	74.7

4.2 Discussion Section

LSWF is an EOR mechanism in which the ion concentration of the injection water is optimized so that it results in an increased oil recovery factor. Some mechanisms are activated when injecting this optimized LSWF water, such as multi-ion exchange, double layer expansion, and mineral dissolution/ precipitation. These mechanisms alter the wettability of the rock to more favorable water-wet conditions and impact the oil reservoir system.

4.2.1 Water optimization (statistical approach)

Two main methods to optimize the ion concentration of the injection water are the: dilution approach and the statistical approach. The statistical tool of the CMG-CMOST software package was used to determine the optimum ion concentration for the injection water. It works so that a random ion concentration distribution is created and compared with other runs until the optimum set of ion concentrations is determined. First, a coarse salinity range was used, and then it was made finer to determine a more accurate optimum injection water.

The optimum ion concentration of the injection water differs depending on the activated mineral and aqueous equations during the LSWF. That is why it is recommended to use the statistical approach rather than the dilution method. Based on the results of simulation of the sandstone core, the reason for the increased recovery during optimized LSWF is because of the reduced number of cations such as (Ca^{2+} and Mg^{2+}) that bridge between the negatively charged sandstone and crude oil, as their concentration reduces the repulsive forces are increasing, and

the oil is desorbed. This was seen when the Ca^{2+} ion was diluted 36.5 times, Mg^{2+} 19 times, and Na^{+} was diluted 3 times; the increase in recovery was 13.4%.

4.2.2 Mineral dissolution/ precipitation

During the optimization of the injection water, an improvement in the connection between the pores (micro and macro) can be observed due to the dissolution of the rock minerals. Mineral dissolution/ precipitation results from the geochemical reactions shown in Equations 3.1- 3.2 and Equations 3.11- 3.12. Calcite is a volatile mineral and can easily dissolve from the formation water (Pouryousefy, et al., 2016). In addition, as a result of lowering the Ca^{2+} ion concentration during the water optimization, the calcium carbonate dissolves and results in the release of the attached crude oil from the rock's surface, which improves the wettability of the rock to more favorable water-wet conditions.

Figure 4.20 and Figure 4.23 show the effect of mineral dissolution and precipitation for both carbonate and sandstone cores, respectively. A positive value reflects the dissolution mechanism in the CMG-GEM simulator, whereas a negative value reflects precipitation. The dominant reaction depends on the saturation index shown in section 2.1.3.1. If the saturation index is > 1, a forward reaction occurs, and the resulting mechanism is the dissolution of the minerals, whereas if the saturation index is < 1, the reaction is backward, and the dominant mechanism is precipitation. As a result of mineral dissolution and precipitation, a change in the porosity and permeability of the rock can be observed and shown in the pore volume change. Based on Equation 3.1, a smaller value of the Ca^{2+} molality will result in precipitation, and the reaction rate would be negative. In contrast, dissolution would occur if the Ca^{2+} molality was bigger, and the reaction rate would be positive. So basically, the higher the molality of the Ca^{2+}, the higher the reaction rate.

The reaction rate of the calcite in the carbonate core is negative, so calcite is dissolving, and not much change is occurring for the dolomite mineral, meaning that the LSWF has a higher impact on the calcite than the dolomite rock. An indication of the precipitation of the calcite is shown in the effluent analysis. When the concentration of the Ca^{2+} ions at the outflow is less than in the inflow, this is an indication of calcite precipitation. If it were to be higher, that's an indication of calcite dissolution.

The timing of the LSWF has a significant impact on all the mechanisms. The earlier it starts and the longer the LSWF occurs, the more time it interacts with the rock and reservoir fluid. Sometimes no porosity or permeability change is observed because LSWF hasn't had enough time to impact the reservoir rock, and no significant pore volume change is observed. At other

times no significant change in the overall pore volume is observed because of the simultaneous effect of mineral dissolution and precipitation; they compensate for one another.

Soleimani et al. (2021) observed that even though micro-changes were occurring to the system's porosity, no macro changes were observed because both mechanisms complemented each other; dissolution increased the minerals' properties, whereas dissolution reduced the minerals' properties. In summary, based on the results of the simulations conducted in this work, mineral dissolution/ precipitation can be combined with other LSWF mechanisms to cause oil recovery improvement.

4.2.3 Multi-ion exchange

Due to the presence of specific ions (Ca^{2+}, Mg^{2+}, Na^{2+}), the ion-exchange process occurs. It results in the shifting of the relative permeability curves and changes the state of the rock to more water-wet (favorable conditions). The ion-exchange equations are shown in Equations 3.10 and 3.15-3.16.

The ion exchange processes are fast and are modeled as chemical equilibrium processes. During the ion exchange process, the oil attached to the rock surface is desorbed (Afekare & Radonjic, 2017). SO_4^{-2} is crucial for the MIE in carbonate rocks. It acts as a surface neutralizing agent that decreases the carbonate surface's positive charge and indirectly expels the absorbed oil, leading to the wettability alteration. Ca^{2+} and Mg^{2+} are crucial in sandstone rock because they bridge between rock surface and oil components. Once LSWF is injected, it makes the DLE increase, increasing the distance between the surface and crude oil resulting in the desorption of the oil. As MIE continues, the oil recovery continues until the maximum CEC value is reached in which no more ions are exchanged, and the oil recovery doesn't increase.

DLE helps the ion-exchange process to occur. The main way to distinguish between the DLE and MIE is to observe the ions involved in the reactions; divalent ions contribute to DLE and MIE, whereas monovalent ions only contribute to the DLE process. Another indication is to observe the effluent ion concentration. Based on published results, a decrease in the effluent Ca^{2+} indicates MIE and precipitation, and an increase in the Ca^{2+} ions indicates dissolution effects (Awolayo, 2014; Chandrasekhar, 2018; Hadi; 2019).

Figure 4.32 and Figure 4.33 show the effect of MIE based on the simulation runs for the carbonate core. MIE is highly dependant on the contrast in compositions of the formation water and injection water. Figure 4.32 shows the molality of Na^+ and Ca^{2+} for the carbonate core. Initially, the formation water has a high Na^+ concentration, but once the LSWF is injected, it causes a disruption in the equilibrium of the rocks system and suddenly reduces the Na^+ value. Figure 4.33 shows the adsorption of the Ca^{2+} ion during the LSWF. Initially, the adsorption

increased because the calcite was dissolving, so as a sudden action, the system compensated for the reduced Ca^{2+} until equilibrium was reached. It shows that less adsorption is occurring. MIE is one of the main mechanisms during LSWF.

In carbonates, SO_4^{-2} impacts the recovery because they are the ions responsible for the ion exchange. In the sandstone, the presence of Na^+, $Ca^{2+,}$ and Mg^{2+} is essential. The ions linked to the crude oil's polar components are accountable for triggering the repulsive forces that expand the double layer. They cause a reduction in the attractive forces between the crude oil and rock surface, resulting in the desorption of crude oil. There is a critical concentration in which, above or below it, the impact of the PDI decreases. The SO_4^{-2} is needed to be present with the Ca^{2+} ions. The adsorption of the Ca^{2+} ion onto the rock surface during LSWF is essential for the attraction of the SO_4^{-2}. It is responsible for the detachment of the Ca-crude oil components. This means that the SO_4^{-2} ion is the main ion responsible for the wettability alteration of the rock (Bai, et al., 2021). For the carbonate core, an oil recovery factor of 65% was obtained at the critical concentration of 47 ppm SO_4^{-2}. Even if the SO_4^{-2} concentration increases, no more incremental oil recovery is obtained because the surface of the rock has reached its maximum CEC (There is no more free surface space to adsorb more SO_4^{-2} ions).

However, for the sandstone core, the impact of the Na^+ ions is important. Based on the study conducted in section 4.1.2.2, the oil recovery factor increased as the Na^+ ions concentration decreased. However, reducing it below 500 ppm did not show any further oil recovery increase because, at that concentration, the ion exchange process, one of the main LSWF mechanisms, will not occur. The most important divalent ions for the sandstone rock are the Ca^{2+} and Mg^{2+}. Because when injected, the LSWF disrupts the rocks system, as the ion composition of the injected water differs from that in the formation water. The presence of the divalent ions (Ca^{2+} and Mg^{2+}) are essential to facilitate the double layer expansion, which is caused due to the increase in the repulsive forces between the rock surface and crude oil components. The expansion of the double layer results in the increased distance between the rock and crude oil results in the release of the absorbed crude oil, and hence oil recovery increase (Elgendy & Porta, 2021). Based on the obtained results, a combination effect of DLE and MIE are the main LSWF mechanisms contributing to oil recovery.

4.2.4 Further Discussion

As discussed in the previous section, the LSWF disrupts the system's equilibrium, resulting in an incremental oil recovery factor, which results in a shift in the wettability of the rock to more favorable conditions. a shift in the relative permeability curves and the crossover point to the right is a good indication. Before LSWF, the crossover was at 0.38, but after LSWF, it reached above 0.55. Another indication of the success is an increase in the endpoint Kro and a decrease

in the Krw. The oil is now more mobile, and the water is less mobile. The outcome is a reduction in the residual oil saturation and an increase in oil recovery.

In the LSWF, the contrast in the composition of the formation water and injection water is essential. Optimization of the injection water based on the mineralogy of the rock can result in the success of the LSWF method. Based on simulation results, the Na^+ and SO_4^{-2} were found to have the highest effect on the sandstone and carbonate, respectively.

CMG-GEM is a good simulator to study the impact and effect of the LSWF on the interactions of the crude-brine-rock system and the oil recovery factor. It was able to investigate the effect of MIE and mineral dissolution/precipitation. However, its deficiency in studying the effect of DLE alone. According to the published results, DLE occurs simultaneously with MIE. As observed in this work, several mechanisms might cause oil recovery to increase.

In the pilot-scale, mineral dissolution was considered an important LSWF that affects the recovery factor. Effluent ion analysis was conducted to get an idea of the impact of the ions in the model. An increase in the Ca^{2+} and Mg^{2+} ions was observed in both fractured and non-fractured homogeneous reservoirs. This could be evidence of mineral dissolution. The pore volume increased between 1.4% in the fractured reservoir and 3.4% in the non-fractured reservoir. The pore volume increase was more pronounced in the homogeneous non-fractured reservoir. This may be because, in the non-fractured reservoir, the movement of the injected LSWF is more consistent and reaches a larger surface area than the case of the fractured reservoir.

Based on the effluent ion analysis, results obtained for the core scale model are different than that of the pilot-scale model. This means that conclusions must not be made based on the results of the core scale data but rather upscaling the model to a pilot model is essential to understand the LSWF mechanisms better.

Chapter 5

Conclusion

The following section presents a summary, evaluation, and future recommended work based on the data used for this study.

5.1 Summary

LSWF is a promising, low-cost, and environment-friendly EOR method for sandstone and carbonate reservoirs implementation. Different LSWF mechanisms have been discussed in the literature, and there is still no evidence of the main LSWF mechanism. However, based on this work, a combination of LSWF results in the wettability alteration and therefore increased oil recovery.

The contrast in the ion composition between the formation water and injection water is important to cause a disruption in the equilibrium of the system and activate the LSWF mechanisms. In the carbonate core, the presence of SO_4^{-2} is important as it acts as a surface neutralizing agent, whereas in the sandstone core, the presence of Na^+ has the highest impact on recovery based on the Sobol analysis conducted in this study.

Optimization of the injection water is proved to be effective in increasing the capability of the LWSF. A combination of different ions was tested through statistical tool application to determine the best effect on oil recovery. This depends on the activated reactions. Recovery is increased when the potential determining ions (PDIs) concentration is reduced in the optimized injection seawater. This is due to the increasing repulsive forces, which lead to crude oil desorption.

An indication of the main mechanism contributing to the oil recovery can be determined based on the effluent ion analysis. Based on the simulation results, an increase in the Ca^{2+} was observed in the effluent, indicating rock dissolution. A decrease in the Ca^{2+} can indicate MIE and rock precipitation. An increase in the Ca^{2+} and Mg^{2+} ions was observed in both fractured and non-fractured homogeneous 5-spot models. This could be evidence of mineral dissolution. In addition, the pore volume increase was more pronounced in the homogeneous non-fractured

reservoir. This may be because, in the non-fractured reservoir, the movement of the injected LSWF is more consistent and reaches a larger surface area than the case of the fractured reservoir. A change in the porosity/permeability and pore volume after LSWF cannot always be observed because mineral dissolution and precipitation can occur simultaneously and compensate for each other. Under certain circumstances, the LSWF might not provide oil recovery enhancement due to the insufficient time for activating the crude oil-rock mechanisms.

Based on the results of the pilot-scale model, the non-fractured system showed a higher recovery factor of 84.8% compared to 76.6% from the fractured reservoir in the heterogeneous case. This is because, in a fractured system, there might be plugged pores that might prevent the reach of the LSWF to the whole fractured network.

When the CEC was reduced from 100 to 50, a 3% oil recovery was observed. This is because the rock dissolves slower. However, in the absence of clay, CEC does not have a big influence on the recovery. The higher the CEC value, the larger the rock's surface area. This also means more time is needed for a system to reach equilibrium.

Optimum recovery factor was observed when the rocks minerals were 50% calcite and 50% dolomite for the carbonate rock. However, in the sandstone core, the presence of clay in the rock mineralogy is important as it gave a 13.3% higher recovery than in the case where no clay was present.

Conclusions about the impact of LSWF mechanisms on recovery should not be made based on core scale data because their results can be misleading. Upscaling to a pilot-scale model is necessary.

Not one LSWF mechanism can be considered the main contributor for wettability change, but a combination of mechanisms might be. The DLE helps the ion exchange process to occur.

5.2 Evaluation

The objectives of this work were met; though, further studies need to be conducted in determining the impact of LSWF on the field scale. In addition, DLE could not be studied alone as CMG shows the final effect of the LSWF and not DLE as a sole mechanism but rather combined with MIE.

5.3 Future Work

Advanced studies of the impact of LSWF on the fractured system in heterogeneous and homogeneous reservoirs should be conducted to understand better the mechanisms as most carbonate reservoirs around the world are fractured. In addition, non-commercial simulation

tools such as DUMu^{x} might be used to investigate the effect of the combination of mechanisms such as DLE and MIE.

Chapter 6

References

Afekare, D. A. & Radonjic, M., 2017. From Mineral Surfaces and Coreflood Experiments to Reservoir Implementations: Comprehensive Review of Low-Salinity Water Flooding (LSWF). *ACS Publications,* pp. 13043-13062.

Akhmetgareev, V. & Khisamov, E., 2015. 40 years of low salinity waterflooding in Pervomaiskoye Field, Russia: Incremental oil. *Society of Petroleum Engineers.*

Austad, T. et al., 2015. Low Salinity EOR Effects in Limestone Reservoir Cores Containing Anhydrite: A Discussion of the Chemical Mechanism. *ACS Publications,* p. 6903–6911.

Awolayo, A., Sarma, H. & Alsumaiti, A. M., 2014. A Laboratory Study of Ionic Effect of Smart Water for Enhancing Oil Recovery in Carbonate Reservoirs. *SPE EOR Conference at Oil and Gas West Asia, Muscat, Oman.*

Bakhshi, P., Kharrat, R., Hashemi, A. & Zallaghi, M., 2017. Experimental evaluation of carbonated waterflooding: A practical process for enhanced oil recovery and geological Co2 storage. *Greenhouse Gases Science and Technology,* pp. 238-256.

Chandrasekhar, S., Himanshu, S. & Mohanty, K. K., 2018. Dependence of wettability on brine composition in high temperature carbonate rocks. Volume 225, pp. 573-587.

CMG Tutorial, 2020.

CMG Tutorials, 2018.

Elgendy, A. M. & Porta, G. M., 2021. Impact of reservoir geochemistry on low salinity waterflooding: Global sensitivity analysis. *Journal of Petroleum Science and Engineering 207.*

Emadi, A. & Sohrabi, M., 2013. Visual Investigation of Oil Recovery by Low Salinity Water Injection: Formation of Water Micro-Dispersions and Wettability Alteration. *SPE Annual Technical Conference and Exhibition, New Orleans, Louisiana, USA,* pp. 1-15.

Esene, C. et al., 2018. Modeling investigation of low salinity water injection in sandstones and carbonates: Effect of Na+ and SO4. *Department of Process Engineering, Faculty of Engineering and Applied Science, Memorial University, St. John's, NL, Canada,* pp. 362-373.

Hadi, Y. A., Hussain, F. & Othman, F., 2019. Low salinity water flooding in carbonate reservoirs – dissolution. *IOP Conf. Series: Materials Science and Engineering 579,* p. 012029.

Hosseini, E., Chen, Z., Sarmadivaleh, M. & Mohammadnazar, D., 2021. Applying low-salinity water to alter wettability in carbonate oil reservoirs: an experimental study. *Journal of Petroleum Exploration and Production volume,* pp. 451-475.

Kafry, L. A., 2020. Mechanistic Study of the Carbonated Smart Water in the Naturally Fractured Reservoir. *Master's Thesis,* p. 79.

Kurgyis, K., 2021. Explicit continuum-scale modeling of water-based IOR/EOR mechanisms. *Doctoral Thesis,* p. 114.

Lee, J. H., Jeong, M. S. & Lee, S. K., 2017. Geochemical Modelling of Carbonated Low Salinity Water Injection CLSWI to Improve Wettability Modification and Oil Swelling in Carbonate Reservoir. *SPE Latin America and Caribbean Mature Fields Symposium, Salvador, Bahia, Brazil.*

Ligthelm, J. D. et al., 2009. Novel Waterflooding Strategy By Manipulation Of Injection Brine Composition. *Society of Petroleum Engineers.*

Mahani, H. et al., 2015. Driving Mechanism of Low Salinity Flooding in Carbonate Rocks. *EUROPEC 2015, Madrid, Spain Society of Petroleum Engineers.*

McGuire, P. et al., 2005. Low Salinity Oil Recovery: An Exciting New EOR Opportunity for Alaska's North Slope. *SPE Western Regional Meeting, Irvine, California.*

Nasralla, R. A. & Nasr-El-Din, H. A., 2014. Impact of cation type and concentration in injected brine on oil recovery in sandstone reservoirs. *Journal of Petroleum Science and Engineering 122,* pp. 384-395.

Nghiem, L., Sammon, P., Grabenstetter, J. & Ohkuma, H., 2004. Modeling CO2 Storage in Aquifers with a Fully-Coupled Geochemical EOS Compositional Simulator. *SPE/DOE Symposium on Improved Oil Recovery, Tulsa, Oklahoma,* pp. 1-16.

Pouryousefy, E., Xie, Q. & Saeedi, A., 2016. Effect of multi-component ions exchange on low salinity EOR: Coupled geochemical simulation study. *Advanced Research Evolving Science,* Volume 2, pp. 215-224.

Sandengen, K., Kristoffersen, A., Melhuus, K. & Josanf, L. O., 2016. Osmosis as Mechanism for Low-Salinity Enhanced Oil Recovery. *Society of Petroleum Engineers,* pp. 1227-1235.

Saw, R. K. & Mandal, A., 2020. A mechanistic investigation of low salinity water flooding coupled with ion tuning for enhanced oil recovery. *RSC Advances,* Volume 10.

Tetteh, J. T., Brady, P. V. & Ghahfarokhi, R. B., 2020. Review of low salinity waterflooding in carbonate rocks: mechanisms, investigation techniques, and future directions. *Advances in Colloid and Interface Science 284,* p. 102253.

Yousef, A. A., Al-Saleh, S., Al-Kaabi, A. & Al-Jawfi, M., 2011. Laboratory Investigation of the Impact of Injection-Water Salinity and Ionic Content on Oil Recovery From Carbonate Reservoirs. *Society of Petroleum Engineers,* pp. 578-593.

Zhang, P. & Austad, T., 2006. Wettability and oil recovery from carbonates: Effects of temperature and potential determining ions. *Colloids and Surfaces A: Physicochemical and Engineering Aspects,* 279(1-3), pp. 179-187.

Zhang, P., Tweheyo, M. T. & Austad, T., 2007. Wettability alteration and improved oil recovery by spontaneous imbibition of seawater into chalk: Impact of the potential determining ions Ca^{2+}, Mg^{2+}, and SO_4^{2-}. *Colloids and Surfaces A: Physicochemical and Engineering Aspects,* 301(1-3), pp. 199-208.